ETSI TR 103 952 V1.1.1 (2025-08)

TECHNICAL REPORT

Smart Body Area Network (SmartBAN); Brain Computer Interface (BCI)

Reference
DTR/SmartBAN-0022

Keywords
device, implant, radio interface

ETSI

650 Route des Lucioles
F-06921 Sophia Antipolis Cedex - FRANCE

Tel.: +33 4 92 94 42 00 Fax: +33 4 93 65 47 16

Siret N° 348 623 562 00017 - APE 7112B
Association à but non lucratif enregistrée à la
Sous-Préfecture de Grasse (06) N° w061004871

Contents

Intellectual Property Rights

Essential patents

IPRs essential or potentially essential to normative deliverables may have been declared to ETSI. The declarations pertaining to these essential IPRs, if any, are publicly available for **ETSI members and non-members**, and can be found in ETSI SR 000 314: *"Intellectual Property Rights (IPRs); Essential, or potentially Essential, IPRs notified to ETSI in respect of ETSI standards"*, which is available from the ETSI Secretariat. Latest updates are available on the ETSI IPR online database.

Pursuant to the ETSI Directives including the ETSI IPR Policy, no investigation regarding the essentiality of IPRs, including IPR searches, has been carried out by ETSI. No guarantee can be given as to the existence of other IPRs not referenced in ETSI SR 000 314 (or the updates on the ETSI Web server) which are, or may be, or may become, essential to the present document.

Trademarks

The present document may include trademarks and/or tradenames which are asserted and/or registered by their owners. ETSI claims no ownership of these except for any which are indicated as being the property of ETSI, and conveys no right to use or reproduce any trademark and/or tradename. Mention of those trademarks in the present document does not constitute an endorsement by ETSI of products, services or organizations associated with those trademarks.

DECT™, **PLUGTESTS™**, **UMTS™** and the ETSI logo are trademarks of ETSI registered for the benefit of its Members. **3GPP™**, **LTE™** and **5G™** logo are trademarks of ETSI registered for the benefit of its Members and of the 3GPP Organizational Partners. **oneM2M™** logo is a trademark of ETSI registered for the benefit of its Members and of the oneM2M Partners. **GSM®** and the GSM logo are trademarks registered and owned by the GSM Association.

BLUETOOTH® is a trademark registered and owned by Bluetooth SIG, Inc.

Foreword

This Technical Report (TR) has been produced by ETSI Technical Committee Smart Body Area Network (SmartBAN).

The contents of the present document are subject to continuing work within the SmartBAN TB and may change following formal TB approval. Should the TB change the contents of the present document, it will be re-released by the TB with an identifying change of release date and an increase in version number as follows:

Version *x*. *y*. *z*

where:

x the first digit:

0: presented to the TB for information.

1: presented to the TB for approval.

2: or greater shows the TB-approved document under change control.

y the second digit is incremented for technical changes, corrections, or updates.

z the third digit is incremented for editorial changes.

Modal verbs terminology

In the present document "**should**", "**should not**", "**may**", "**need not**", "**will**", "**will not**", "**can**" and "**cannot**" are to be interpreted as described in clause 3.2 of the ETSI Drafting Rules (Verbal forms for the expression of provisions).

"**must**" and "**must not**" are **NOT** allowed in ETSI deliverables except when used in direct citation.

Executive summary

The present document lays out an outlook for the Brain-Computer Interface (BCI) use case with an invasive ECoG implant and an interface for Wireless Power Transfer (WPT) and data communications. Coping with the high throughput required to capture large portions of the brain, THz technology is presented as a potential new healthcare vertical for future wireless systems, such as 6G and an extension of SmartBAN networks.

1 Scope

The present document is limited to providing information for the brain computer interface use case.

The present document discusses proof of concept in the design of the wireless interface for the next-generation of μECoG electrode arrays implanted in the human brain. This includes recording and stimulation of large regions of the brain at a high spatial resolution, as well as energy harvesting, power management, and data communications processing. In particular, the present document focuses on the wireless communication interface.

2 References

2.1 Normative references

Normative references are not applicable in the present document.

2.2 Informative references

References are either specific (identified by date of publication and/or edition number or version number) or non-specific. For specific references, only the cited version applies. For non-specific references, the latest version of the referenced document (including any amendments) applies.

NOTE: While any hyperlinks included in this clause were valid at the time of publication, ETSI cannot guarantee their long-term validity.

The following referenced documents may be useful in implementing an ETSI deliverable or add to the reader's understanding, but are not required for conformance to the present document.

[i.1] ETSI TR 138 901 (V16.1.0): "5G; Study on channel model for frequencies from 0.5 to 100 GHz (3GPP TR 38.901 version 16.1.0 Release 16)".

[i.2] T. Nagatsuma, et al.: "Advances in terahertz communications accelerated by photonics", Nature Photonics, vol. 10, pp. 371 to 379, 2016.

[i.3] R.B. Reilly: Neurology: central nervous system, in: J.G. Webster (Ed.), "The Physiological Measurement Handbook", CRC Press, New York, 2014.

[i.4] R. Muller et.al.: "A minimally invasive 64-channel wireless μECoG implant", IEEE Journal of Solid-State Circuits 50 (1) (2015).

[i.5] P.P. Mercier, A.P. Chandrakasan (Editors.): "Ultra-Low-Power Short-Range Radios", Springer, 2015.

[i.6] IEC/IEEE™ 62209-1528: "Measurement procedure for the assessment of specific absorption rate of human exposure to radio frequency fields from hand-held and body-worn wireless communication devices".

[i.7] R. Kankula: "Advances in hardware systems for implantable medical devices: challenges and opportunities", International Research Journal of Modernization in Engineering Technology and Science 7(3):2582-5208.

[i.8] Basabi, Inokawa, Roy (Editors): "Terahertz Biomedical and Healthcare Technologies", 2020, Elsevier.

[i.9] Kürner, Mittleman, Nagatsuma (Editors): "THz Communications Paving the Way Towards Wireless Tbps", 2022, Springer.

[i.10] World Radiocommunication Conference 2023 (WRC-23) Final Acts.

[i.11] IEEE Std 802.15.3™-2017: "IEEE Standard for High Data Rate Wireless Multi-Media Networks".

3 Definition of terms, symbols, and abbreviations

3.1 Terms

For the purposes of the present document, the following terms apply:

craniotomy: surgical removal of a portion of the skull

energy scavenging: conversion of ambient energy present in the environment into electrical energy for use in powering electronic devices or circuits

3.2 Symbols

Void.

3.3 Abbreviations

For the purposes of the present document, the following abbreviations apply:

AP	Access Point
BCI	Brain-Computer Interface
BER	Bit Error Rate
EAP	Extracellular Action Potentials
ECoG	Electrocorticography
EEG	ElectroEncephaloGraphy
MEG	Magneto-Encephalon-Graphy
MRI	Magnetic Resonance Imaging
NFC	Near-Field Communication
PET	Positron Emission Tomography
QCL	Quantum Cascade Laser
RF	Radio Frequency
RTD	Resonant Tunneling Diodes
SAR	Specific Absorption Rate
THz	Tera Herz
UTC-PD	Uni-Traveling-Carrier Photodiode
WPT	Wireless Power Transfer

4 BCI overview

The use case of BCI targets the development and application of innovative neural technologies to advance the resolution of neural recording and stimulation toward the dynamic mapping of brain activity and neural processing. These advanced neuro-technologies will enable new studies and experiments to advance the current understanding of the brain. Hence, enabling advances in diagnosis and treatment opportunities over a broad range of neurological diseases and disorders, as well as commercial applications.

Studying the dynamics and connectivity of the brain requires a wide range of technologies to address temporal and spatial resolutions. Figure 1 shows such spatial and temporal resolutions in the function of various brain monitoring technologies that are currently available [i.3].

Noninvasive methods such as Magnetic Resonance Imaging (MRI), Functional Magnetic Resonance Imaging (FMRI), Magneto-Encephalon-Graphy (MEG), and Positron Emission Tomography (PET) provide whole-brain spatial coverage:

- FMRI provides high spatial resolution (around 1 mm), but its temporal resolution is limited (1 sec to 10 sec) for the system measuring neural activity.
- MEG provides higher temporal resolution (0,01 sec to 0,1 sec) at the expense of spatial resolution (1 cm).

- PET offers molecular selectivity in functional imaging at the expense of lower spatial (1 cm) and temporal (10 sec to 100 sec) resolutions. However, neither FMRI, MEG, nor PET is suitable for wearable or portable applications, as they all require very large, expensive, and high-power equipment to support the sensors, as well as extensively shielded environments.

In contrast, electrophysiology methods that directly measure electrical signals from the neurons' activity offer superior temporal resolution. They have been extensively used to monitor brain activity due to their ability to capture wide ranges of brain activities from the subcellular level to the whole brain oscillation level as shown in Figure 1.

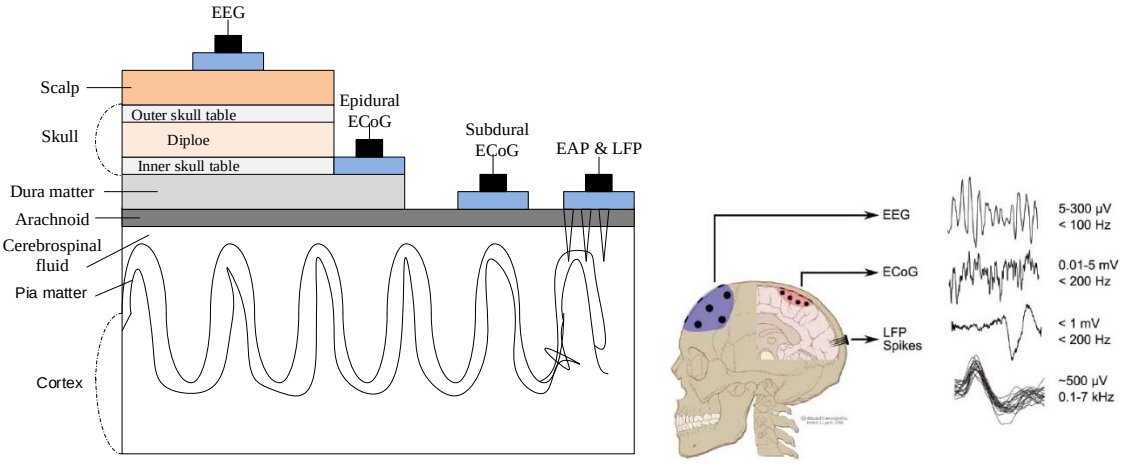

Figure 1: Illustration of electrophysiology methods

Due to recent advances in electrode and integrated circuit technologies, electrophysiological monitoring methods have become portable with wearable or implantable configurations for BCI. In particular, Electro-Encephalography (EEG) records the electrical activity on the scalp resulting from volume conduction of neural activity across the brain, as shown in Figure 1. Moreover, EEG recording is noninvasive, but its spatiotemporal resolution is limited to about 1 cm and 100 Hz due to the electrical properties of diverse layers of head and brain tissues, particularly the skull (between the brain and the scalp).

In contrast, microelectrodes technology such as Extracellular Action Potentials (EAPs) and Local Field Potentials (LFPs) enable recording from multiple neurons across multiple cortical areas and layers. Those can achieve much higher resolution because of the closer proximity to individual neurons. Hence, EAP+LFP techniques are widely used for brain research and BCI applications.

On the other hand, microelectrodes may suffer from tissue damage during insertion and be susceptible to signal degradation due to electrode displacement over time and an immune response against the electrodes. Because of these issues, penetrating microelectrodes in humans are not yet viable.

A practical alternative is electrocorticography (ECoG), or intracranial/intraoperative EEG (iEEG), which records synchronized postsynaptic potentials at locations much closer to the cortical surface, as illustrated in Figure 1. Figure 2 illustrates the deployment of ECoG devices.

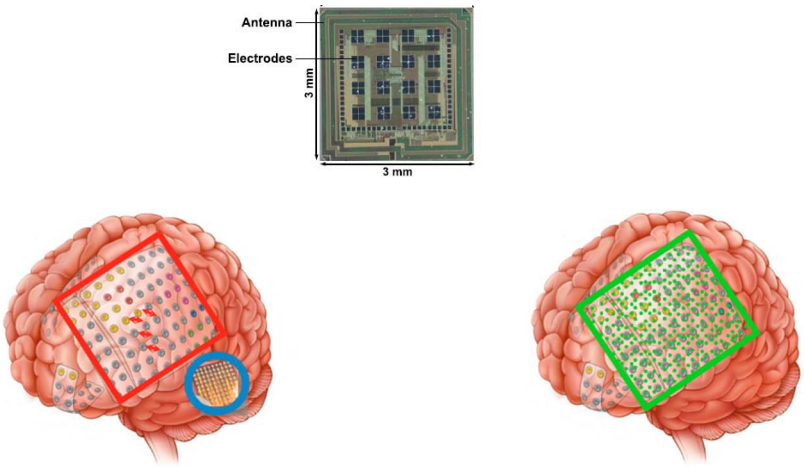

Figure 2: Illustration of ECoG devices and deployment in the brain

ECoG has a higher spatial resolution than EEG, a higher signal-to-noise ratio, broader bandwidth, and much less susceptibility to displacement. Furthermore, ECoG does not penetrate the cortex, does not scar, and can have superior long-term signal stability recording. Furthermore, advances in integrated circuits that enable high channel count and wireless operation, ECoG has become an important tool not only for more effective treatment of neurological disorders, like epilepsy, but also for investigating other types of brain activity across the cortical surface, and its applications to BCI systems.

ECoG recording provides stable brain activity recording at a mesoscopic spatiotemporal resolution with a large spatial coverage, or at least a significant area of the brain.

Advanced and miniaturized electrode arrays have reached a spatial resolution of less than 1 mm, enabling monitoring of large-scale brain activity with greater accuracy. Moreover, wireless implantable microsystems based on flexible technology can record more closely to the cortical surface while enabling coverage along the natural curvature of the cortex without penetration as shown in Figure 3.

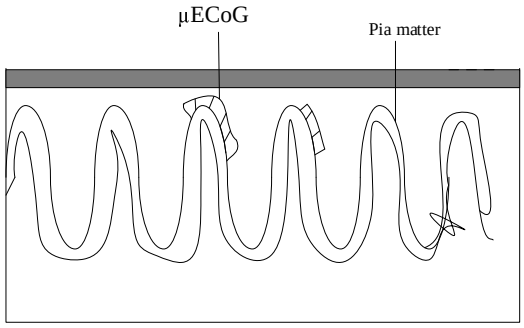

Figure 3: Implantable µECoG on flexible substrate

This ECoG technology, labeled as µECoG, enables even higher spatial resolution than conventional ECoG systems and is beginning to enable next-generation brain mapping, therapeutic stimulation, and sophisticated BCI systems.

Therefore, recording with modern implementations of ECoG arrays falls into one of two categories:

1) Medium-size brain regions (about 80 mm × 80 mm) at a low spatial resolution of 10 mm electrode spacing for conventional ECoG.

2) Small brain regions (10 mm × 10 mm) at high spatial resolution (0,5 mm to 1 mm electrode spacing): µECoG.

The present document discusses the design of the wireless interface for the next-generation of µECoG electrode arrays, illustrated in Figure 4, including recording, stimulation of large regions of the brain at a high spatial resolution, as well as energy harvesting, power management, and data communications processing. In particular, the present document focuses on the wireless communication interface, including cybersecurity and privacy protection.

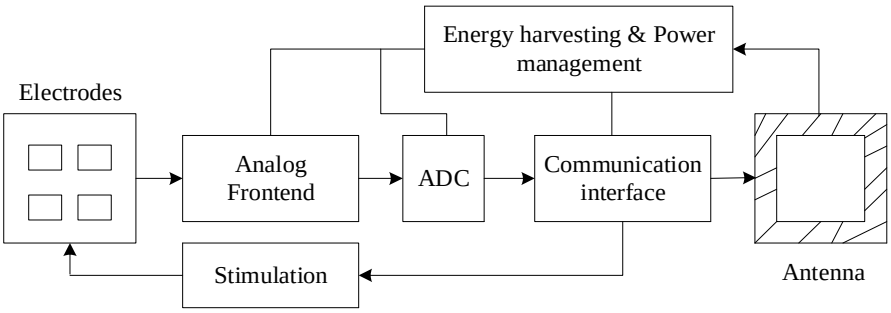

Figure 4: Schematic diagram of functional blocks for BCI node

Neural data acquisition with a high spatial resolution requires a high channel density of ECoG arrays and, consequently, smaller electrode size. If the area overhead of the Application-Specific Integrated Circuits (ASICs) should be kept small, then the area dedicated to the functions illustrated in Figure 4 (amplify and digitize each channel) should reduce as well.

However, a denser array of amplifiers in the Analog Frontends (AFE) will dissipate more power and generate more heat. Thus, the power of each AFE is reduced to meet thermal regulatory limits [i.6].

Unfortunately, as the signal power decreases, the Signal-to-Noise Ratio (SNR) also decreases, affecting the transmission or reception performance requirements for wireless signals.

On the other hand, a higher channel count requires higher communication throughput, increasing the power consumption and heat dissipation of the communication interface. All these requirements are interrelated and trade-off with each other.

In addition, there are several circuit designs challenges, like high power Supply Rejection Ratio (PSRR), difficulty in using external components such as inductors or capacitors. However, these are not addressed in the present document.

Another topic not addressed in the present document is interfaces for stimulation.

5 BCI system considerations

5.1 Energy source

5.1.0 Introduction

The constrained environment around the brain presents an energy source challenge. Indeed, one of the major challenges on implantable μECoG arrays for BCI nodes is how to power such implantable devices.

Even logistically, it is an issue. For example, the electrode array is placed on the cortex, while the other components are placed under the scalp, connected with lead wires or better mounted over a titanium plaque that replaced part of the skull by a craniotomy, eliminating the risk of infection by the lead wires.

Regardless of placement, the constrained environment around the brain presents an energy source challenge. There are three primary methods for powering an implanted device:

1) use a battery;
2) harvesting energy from the environment;
3) delivering power transcutaneous via a wireless power transmitter.

5.1.1 Battery

Another implantable application such as pacemakers has used batteries extensively. However, it makes sense to use a battery in a pacemaker, because the required power is relatively small (microwatts) and there is a large physical area available such that a battery can last 10 years or more.

In contrast, the power consumption in high-density neural recording and stimulation applications is typically much larger (milliwatts), and the physical volume available for a large battery is very small, making it unfit.

Another important aspect is that going through surgical re-implantation to replace a battery is unacceptable to most patients. The medical risks of regular brain surgery and recovery disqualify batteries from being employed in high-density neural applications.

5.1.2 Energy harvesting

Harvesting energy from ambient sources in local environments has been studied as a potential power source option. Some scavenging methods include solar cells, biofuel cells, thermoelectric generators, piezoelectric generators, and ambient RF.

While such approaches are theoretically attractive for implant neural devices, the limited area available near the brain and the stochastic nature of many energy harvesting sources result in a power source that is too small and too variable to operate multi-channel neural technologies.

5.1.3 Wireless power transfer

The most promising means to power an implanted device with higher power requirements than pacemakers is to deliver energy wirelessly via a transcutaneous link, also known as Wireless Power Transfer (WPT).

A transcutaneous link may use light (typically near-infrared light), or acoustics (typically at ultrasound frequencies), or electromagnetic waves (obviously not in the light range). Each method can deliver from μW to mW of energy power. However, such delivered energy depends on the geometry, make-up, implant depth, and orientation of the receiving transducer.

On the other hand, WPT via infrared light has a short penetration depth (around mm), limiting its utility to subcutaneous implant applications. Ultrasound can penetrate deeper into tissues. However, it is known that ultrasonic energy does not efficiently penetrate bone, limiting opportunities to directly power cortical implants from outside the skull. Therefore, the most promising transcutaneous power delivery approach utilizes electromagnetic waves.

Electromagnetic waves in the near- or mid-field is generally considered the most efficient and practical WPT method for such devices implanted a few cm. Therefore, most conventional designs for implant medical devices operate in the near-field between 120 MHz and 20 MHz (conductivity and losses in tissue increase at higher frequencies). Moreover, operating at higher frequencies is constrained by government regulations that limit the amount of dissipated power in tissues for safety reasons. For example, the FCC sets a Specific Absorption Rate (SAR) of less than 1,6 W/kg in the USA. For these reasons, conventional transcutaneous power transfer links operate in the low-MHz range.

However, recent advances in small coil antennas show that the antenna's quality factor and radiation resistance increase with frequency. Thus, μECoG devices with small coils as transducers for WPT would perform better at higher frequencies. Moreover, the trade-off between frequency of operation and tissue heat-up shows that it is possible to deliver mW of power to small, implanted WPT antennas under regulatory limits [i.5], [i.6]. Thus, radio electromagnetic approaches are the primary means to deliver power to implanted ECoG devices.

5.2 Communication interface

5.2.0 Introduction

ECoG devices convey the acquired data to an external controller or Access Point (AP) via a wireless link, where the information can be processed and monitored for diverse applications from healthcare providers to scientific research.

In contrast to conventional star topologies, an ECoG network supports more traffic (aggregated throughput) from a number of ECoG devices to the AP in the uplink (device to AP), than the downlink (AP to device). Moreover, the uplink aggregated data rate may be relatively high (in the order of Mb/s), and subject to stringent power consumption constraints, especially when the number of electrodes (channels) increase significantly.

The radio waves for the uplink may be in the near-field or far-field, depending on the application. Assuming the AP is mounted on goggles, the radio link is in the near-field, while if the AP is at a distance of more than 1 m, the radio link is in the far-field. SmartBAN was designed to operate in the far field. However, it will not require much modification to the MAC layer, but would require a new PHY to cope with near-field protocols for communication and WPT at a higher frequency.

The current state-of-the-art of wearable radios, like Bluetooth® Low Energy, require more than 1 nJ/bit [i.7], which is larger than what a typical ECoG device uses. Hence, the design problem is divided into two categories: research directions in THz spectrum, and a transition phase.

An intermediate transition phase assumes one fusion center mounted on a titanium plaque implanted on the skull. Such fusion center can connect ECoG devices implanted on the brain without the radio interface via cables. Hence, the aggregated throughput is centralized in one unit, which is not close to the brain tissue and consequently tolerate a bit more heat-up.

A candidate is UWB technology. UWB enables low power consumption (around pJ/bit). However, due to government regulatory constraints, the allocated UWB band varies from country to country, and it is not possible to operate a system in the range 3,1 GHz to 10 GHz anymore. However, a UWB system design in the high band of UWB may be worth studying.

5.2.1 Backscatter communication in the near field

Near-field communications operate at distances about one wavelength of the carrier frequency. Hence, it is suitable when the AP is located on the head, for instance, on virtual reality goggles. In addition, WPT can be integrated easily.

Regarding the WPT for the downlink (AP to device), the backscattering method is one of the most popular. Backscattering is a technique to transfer power wirelessly from a transmitter to a receiver by modulating the impedance of the receiver's antenna such that the Electromagnetic Wave (EW) from the transmitter gets more absorbed at the receiver's antenna or more reflected back to the transmitter. The principle is that the reflected EW from the receiver modulates the information bits using a switch. In that manner, the power consumption on the ECoG's communication block is minimal (around pJ/bit), as conventional modulation is not used.

However, the data reception of the reflected EW at the transmitter depends on the power of such backscattered signal, which in turn depends on the system design and distance between transmitter and receiver. Backscattering is best suited for applications where low to moderate power transfer is sufficient and energy efficiency and passive operation are priorities.

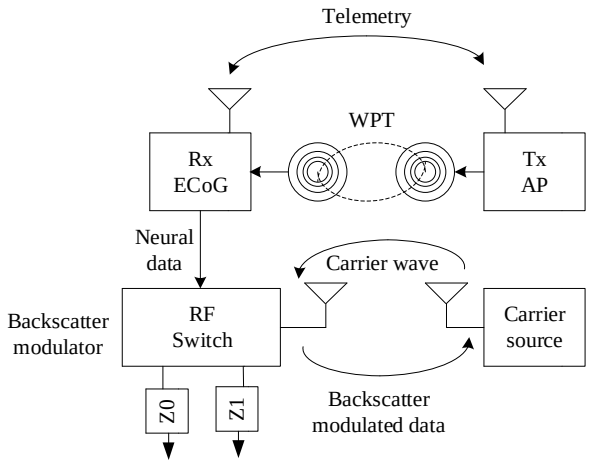

Figure 5: Schematic diagram of backscatter communication

5.2.2 ECoG wireless links

The processing, power, and size-constrained ECoG devices lead toward short-range wireless links. Moreover, ECoG devices typically have a depth of a few cm and high-throughput neural recording. Hence, WPT is a natural choice as the primary mode of power transfer due to its high efficiency and robustness in comparison to ultrasound and energy harvesting.

Thus, over the years, inductive power transfer has been the focus of studies resulting in the development of many efficient designs and methodologies. Moreover, Near-Field Communication (NFC) using inductive links offers a lower cost of communication than far-field communication methods, and it has become the primary means of communication.

ECoG devices may be arranged with three configurations: an entire device placed on the cortex, an electrode array placed on the cortex with an interface on the craniotomy, or placed under the scalp. In these configurations, the location of such devices results in a challenge for WPT and data communication, besides the constrained power consumption and asymmetric traffic requirements as illustrated in Figure 6.

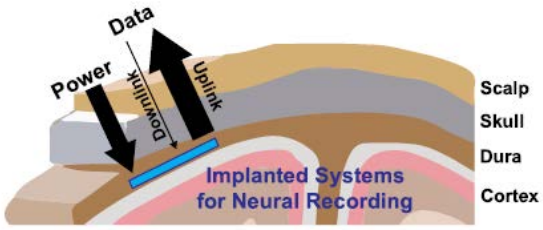

Figure 6: Simplified illustration of an ECoG and requirements for WPT and data communication

To have an idea of the throughput requirements, it is assumed an ECoG recording with 1 024-channels with a sampling rate of 600 samples/s per channel and a data resolution of 10 bits, requires 6,15 Mb/s. Similarly, 64-channels recording with 10 000 samples/s rate and 10-bit resolution, requires 6,4 Mb/s.

State-of-the-art implant devices transmitting at these data rates typically consume several mW [i.7]. Moreover, the position of the ECoG's antenna on the brain tissue has an impact on the WPT and communication link requirements. Figure 7 shows options for implementation:

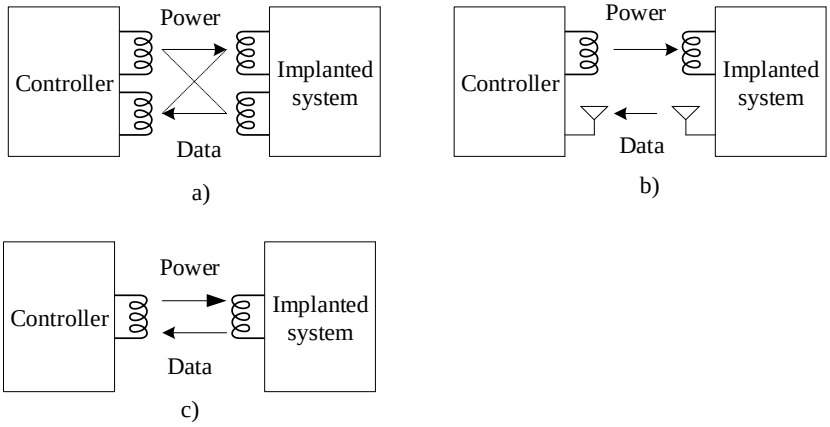

Figure 7: Radio interfaces for WPT and data communication

- Inductive links for power and data communication are shown in Figure 7a). The links are optimized independently. Hence, the configuration enables a high data rate while maintaining high power transfer efficiency. However, this approach requires a more complicated antenna structure and suffers from crosstalk.
- Using different and distinct Radio Frequency (RF) bands as shown in Figure 7b). The scheme can achieve the required data rate. However, it may require more energy for data communications and increased complexity.
- A simple approach uses a single inductive link to transfer both power and data, as illustrated in Figure 7c). Typically, backscattering is used for passive data communication.

5.3 Body Tera Hertz networks

5.3.0 Introduction

Covering significant portions of the brain with an adequate sampling resolution will require a high throughput to be handled adequately for one central unit with significant processing and power constraints.

Therefore, researching the use of THz technology for WPT and data communication is due to the recent advances in the field.

Figure 8 shows classifications of the THz band. From the RF spectrum perspective, THz frequencies start at 100 GHz (0,1 THz), while from an optical communication perspective, the THz band is below 10 THz (the far-infrared spectrum). Most publications are within this spectrum range.

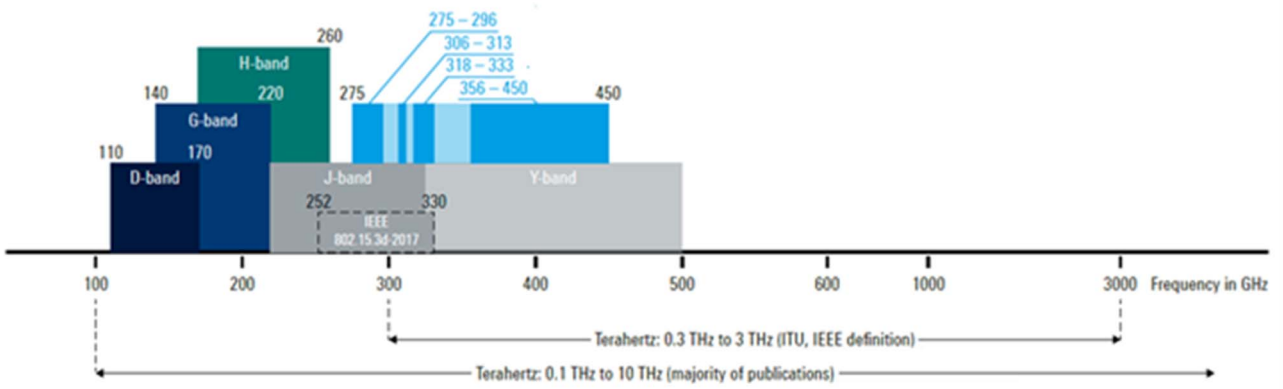

Figure 8: THz frequency bands

Some medical applications already use the THz band, such as in oncology and medical imaging. Due to the short-range connectivity, small form factor, and wide available bandwidth, the THz band enables connectivity of in-body wireless networks. Moreover, THz radiation is relatively safe on biological tissues [i.8]. Hence, the THz spectrum can improve the performance of existing Body Area Networks, enabling various medical applications. In particular, a THz-based network can operate inside the human body in real-time for health monitoring and medical implant communication. Therefore, THz technology is very attractive for the next generation of BCI.

NOTE: THz systems have been associated with the operation of nano-machines and interaction with so-called molecular communications. However, the present document does not consider these applications, but rather the potential use of radio interfaces for WPT and communication of high throughput data in a small form factor and efficiency, which are closer to practical implementations.

Indeed, the proposed BCI use case and the use of THz bands may be seen as part of the key enablers for 6G next generation of wireless communications, as it enables E-health, besides of fully merged virtual worlds, mixed reality and immersive events, like sports, entertainment, gaming, work, social networks.

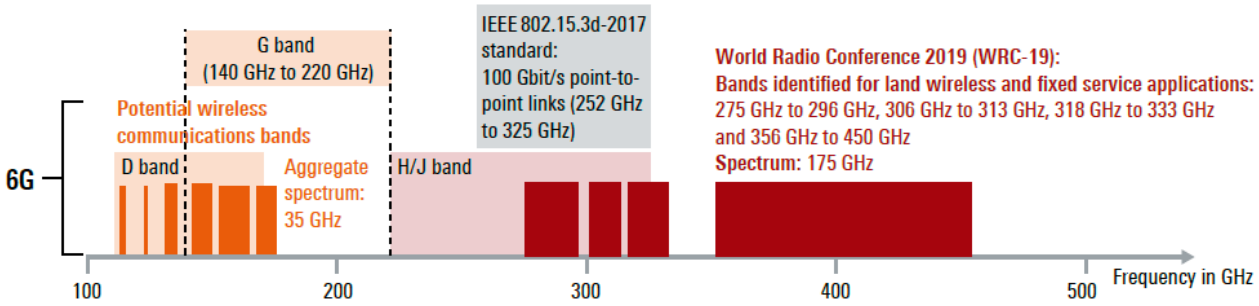

Figure 9: THz band from a 6G perspective

5.3.1 Enhancements to channel modeling

THz technologies still face various challenges. Among others, the propagation characteristics of THz channels.

Contributions describing THz channel measurements and modeling indicate [i.9]:

- Path loss and shadowing (large-scale) parameters in THz bands exhibit specific features compared to frequencies below 100 GHz. THz waves suffer much higher free space path loss when compared to mm-wave and lower frequencies. Moreover, its properties of penetration, diffraction, and scattering are different.
- Similarly, small-scale (fast-fading) parameters are also unique to the THz band [i.2].
- Furthermore, molecular absorption and the effect of changing ambient conditions, like humidity, cannot be neglected in the case of THz channels [i.2].

THz wavelengths are small compared to mm-wave wavelengths, resulting in a reduction of the effective aperture antenna. Hence, a THz antenna array would be attractive to implement in the uplink receiver:

- However, this means that the Rayleigh distance (the conventional boundary between the near field and far field) may be larger than the communication range, and then spherical wave modeling is required [i.2].
- On another hand, the spatial non-stationarity (antenna elements at different spatial positions may capture different multipath characteristics) may need to be modeled for the THz bands as the antenna array aperture may be larger relative to the wavelength [i.2].

5.3.2 Electronic and photonic technologies

5.3.2.0 Introduction

THz bands are promising candidates for future radio systems due to potential applications beyond high data rate capacity, such as integrated sensing and imaging. However, it has been difficult to generate intensive, directional THz radiation. Figure 10 shows the emission power vs. frequency for various electronic and photonic devices, which illustrates the power drop around the THz spectrum.

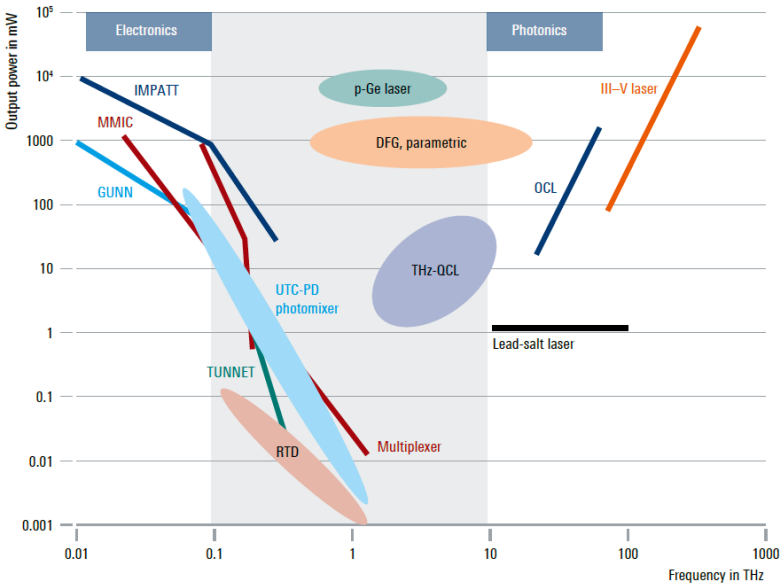

Figure 10: Electronic and photonic devices output power vs frequency

THz frequencies are too high for electronic devices, mainly due to excessive loss and limited high-mobility semiconductor materials. On the other hand, they are too low for photonic devices due to the lack of materials with a sufficiently small bandgap [i.4]. The emission power around the THz region is lower than in other spectral regions. However, for the BCI use case, this is not a disadvantage, as the communication distances are short.

5.3.2.1 Electronic sources

Electronic sources have advanced in the past years, especially with the refinement of various semiconductor materials. For example, frequency multiplier chains with Resonant Tunneling Diodes (RTD). However, still they have certain limitations in bandwidth and efficiency.

5.3.2.2 Photonic sources

There are two methods of generating THz radiation using photonic devices:

- Direct THz generation with optical sources includes the Quantum Cascade Laser (QCL) or nonlinear optics that directly generate THz radiation. Reasonable power levels can be reached with QCL, but the efficiency is still limited as they operate at cryogenic temperatures.
- Indirect THz generation involves one or more devices oscillating at a much higher frequency (typically infrared or optical) along with a nonlinear mixing device. Indeed, the output of two continuous-wave single-mode lasers with closely spaced emission frequencies, ν1 and ν2, respectively, is mixed in an ultrafast photodetector, inducing a photocurrent modulated at the optical frequency of ν = ν1–ν2 in the THz region. The photo mixing technique has the advantage that tuning the lasers is relatively easy with current technology, and consequently, the difference frequency can be varied over a broad spectral range, or highly tunable THz radiation.

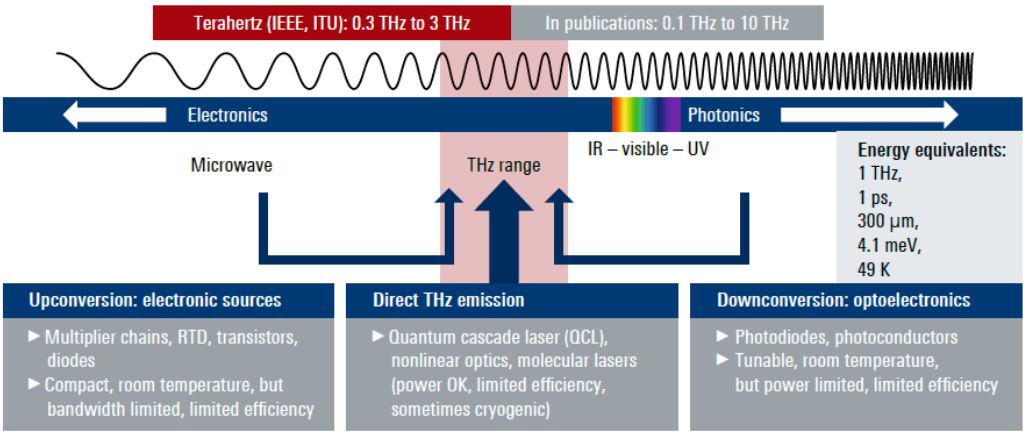

Figure 11: Sources of THz radiation

6 Design considerations

6.0 General

To continue the development of BCI wireless applications, it is explored the feasibility of [sub] THz technologies for wireless data signaling and WPT as follows:

- Selecting the [sub] THz spectrum of interest.
- Experimental studies to determine Specific Absorption Rate (SAR) and propagation effects of [sub] THz radiation on animal tissues (In vitro studies on swine tissues). To indicate the limits of THz radiation on proxy-human tissues on wearables and implants.
- Literature research on promising hardware technologies in the THz regime.
- Design of a Body-Centric network.

6.1 Selecting THz frequency bands

6.1.1 General

Due to the wide frequency range for the THz band, practical application for BCI is likely to use a subband. Hence, selecting THz frequency bands is an important design item.

An overview of the process taken by ITU during the World Radiocommunication Conference of 2023 (WRC-23) is important as it impacts radio regulation across the World and is relevant for THz communications in selecting the appropriate frequency band for BCI applications. The present document briefly describes the corresponding outcomes mentioned in the "WRC-23 Provisional Final Acts [i.10]".

As mentioned in Figure 8, the frequency range for THZ is identical to the bands defined in IEEE Std 802.15.3-2017 [i.11] with the addition of a new frequency band allocation and calls for studies and considerations for new allocations that can be potentially used for THz technologies.

6.1.2 WRC-23 AI 1.14

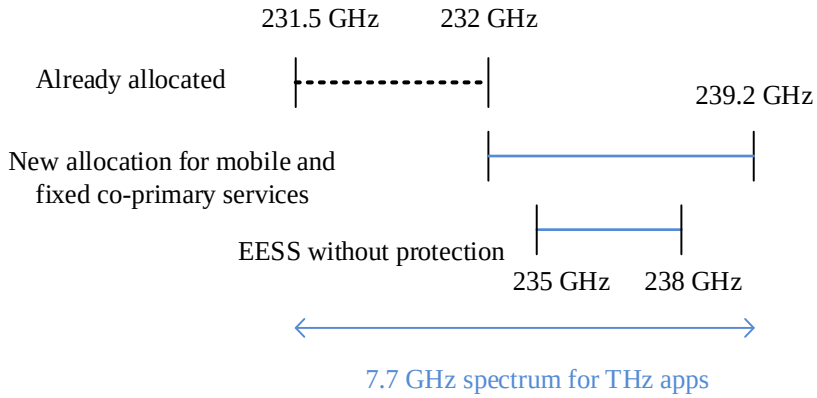

Figure 12: Outcome AI 1.14

a) The new spectrum allocation between 232 GHz and 239,2 GHz has been allocated for mobile and fixed services on a co-primary basis.

b) A new FN (5.B114) has been added: In the frequency band 235 GHz to 238 GHz, stations for Earth Exploration-Satellite Service (EESS) passive does not claim protection from stations in fixed and mobile services.

An additional 7.7 GHz spectrum is available for THz technologies, fixed or mobile.

6.1.3 WRC-27 AI 1.8

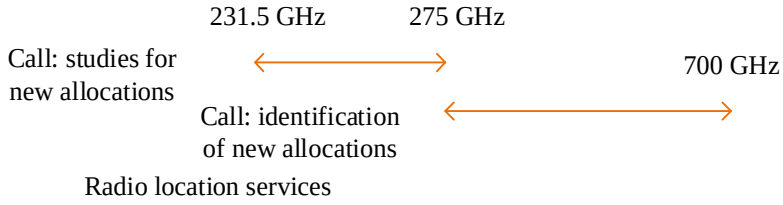

Figure 13: Outcome of AI 1.8

a) Resolution 663 (Rev. WRC-23 [i.10]) discusses studies of possible new allocations in the frequency band 231,5 GHz to 275 GHz and identifications for radio location services in 275 GHz to 700 GHz.

From the previous clause, studies for mobile and fixed services with radio location services in such THz band.

6.1.4 WRC-23 resolution 731

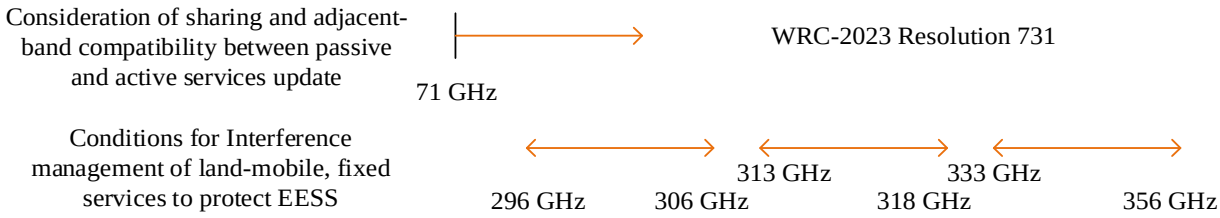

Figure 14: Outcome resolution 731

a) Resolution 731 (Rev. WRC-23 [i.10]): "Consideration of sharing and adjacent-band compatibility between passive and active services above 71 GHz" was updated.

b) Call to conduct studies to determine the specific conditions to be applied to the land-mobile and fixed services to ensure the protection of EESS (passive) applications in the frequency bands 296 GHz to 306 GHz, 313 GHz, 318 GHz, and 333 GHz, 356 GHz.

6.1.5 WRC-31 Potential New AI

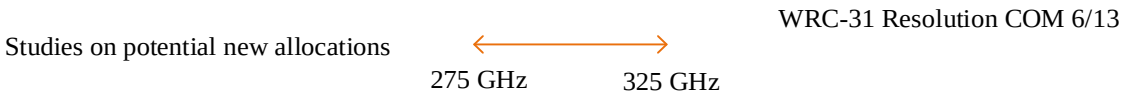

Figure 15: Outcome resolution com 6/13

a) Resolution COM 6/13 (WRC-23 [i.10]): Studies on potential new allocations for fixed, mobile, radiolocation, amateur, amateur-satellite, radio astronomy, Earth exploration-satellite (passive and active), and space research (passive) services in the frequency range 275 GHz to 325 GHz.

b) The corresponding studies are requested to be completed by WRC-31.

WRC-23 outcomes give a starting point to perform experimental research for THz technologies applied to BCI.

6.2 Photonic technology in THz transmission

6.2.1 Overview

Future wireless systems require high wireless data communication capacity that involves immersive virtual and extended reality, as well as medical applications in BCI use cases. Figure 16 shows persons with goggles, but the aim of future BCIs is for headbands or glasses.

Figure 16: Immersive virtual and extended reality

As stated in the previous clause, THz supports high bandwidth allocation that can enable BCI use cases. However, electronics for THz transmissions are difficult to produce as it touches the limits of conventional semiconductors. Hence, an attractive approach is to use photonic technology, which is mature enough, and down-convert somehow.

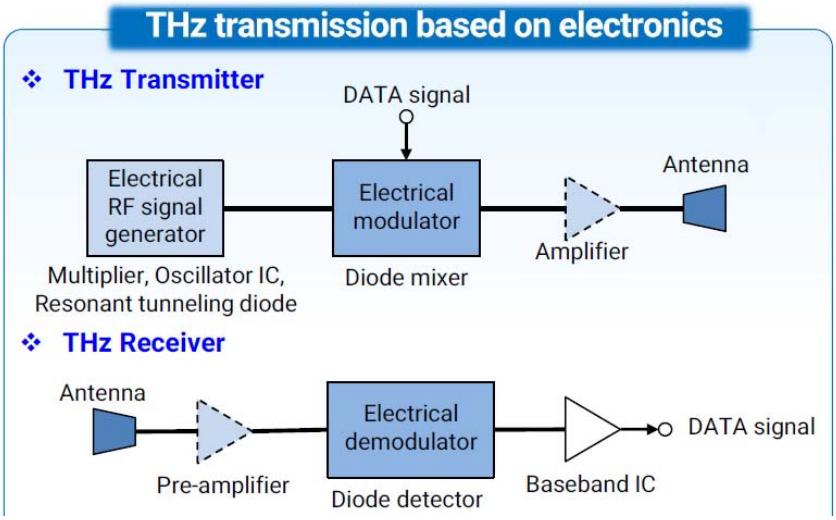

Figure 17: THz transceiver

Figure 17 shows the conventional architecture of a THz transceiver.

1) Available frequency < 300 GHz (III-V & Si)

NOTE: III-V semiconductors are created through the combination of elements from group III (like Gallium, Aluminium, and Indium) and group V (including Phosphorus, Arsenic, and Nitrogen).

2) Maximum data rate: 120 Gb/s (III-V & Si) @ 300 GHz

3) Maximum transmission distance: 10 m @ 300 GHz (III-V, 50 dBi antenna + THz amp)

4) Easy to miniaturize, and integrate, low-power consumption.

5) Matured III-V semiconductor fabrication process.

6) Significant SNR degradation caused by the frequency multiplier chain.

Figure 18 shows a photonic-based THz transceiver.

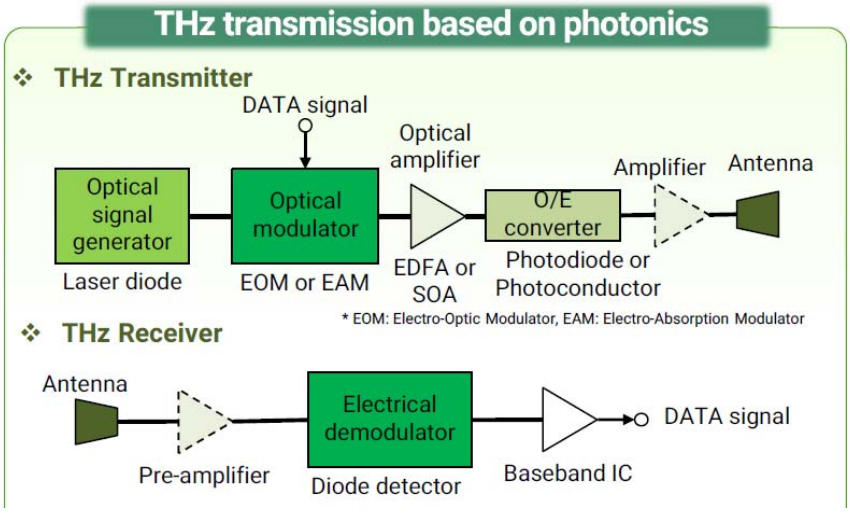

Figure 18: Photonic-based THz transceiver

1) Available frequency < 1 THz.

2) Maximum data rate: 110 Gb/s (Single channel), 600 Gb/s (Multi-channel, PDM) @ 300 GHz.

3) Maximum transmission distance: 110 m @ 300 GHz with THz amp.

4) Matured optical communication technology.

5) Enable high SNR (extended coverage).

6) Difficult to miniaturize, integrate, and achieve low-power consumption.

Figure 19 illustrates different technologies proposed for THz transmission based on photonics.

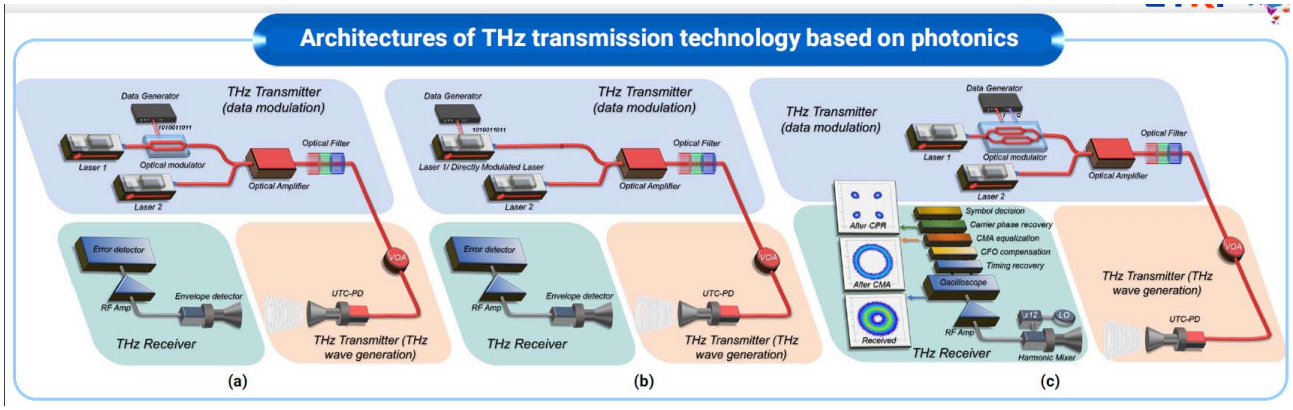

Figure 19: THz transceiver architectures:
(a) External modulation/incoherent
(b) direct modulation/incoherent detection
(c) Optical IQ modulation/coherent detection

6.2.2 Technical challenges

A popular approach is to use InP/InGaAs Uni-Traveling-Carrier Photodiode (UTC-PD) to generate THz signals. However, a known technical challenge is the generation of output power to compensate for THz attenuation, Figure 20. Another technical challenge is the miniaturization and integration in a small form factor fabrication process, Figure 21.

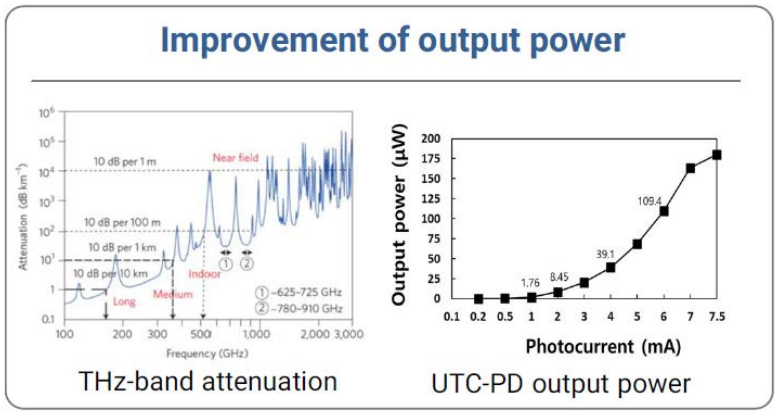

Figure 20: Generation of sufficient output power challenge

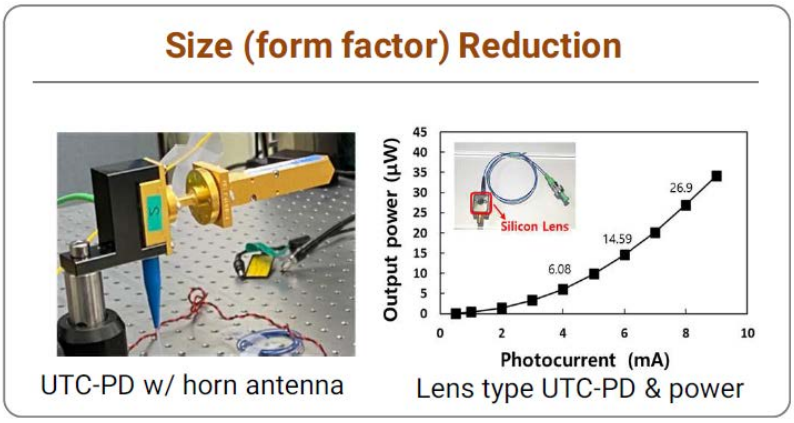

Figure 21: Miniaturization and integration challenges

Recent advances in UTC-PD lithography show the achievement of high bandwidths in a relatively small area, Figure 22.

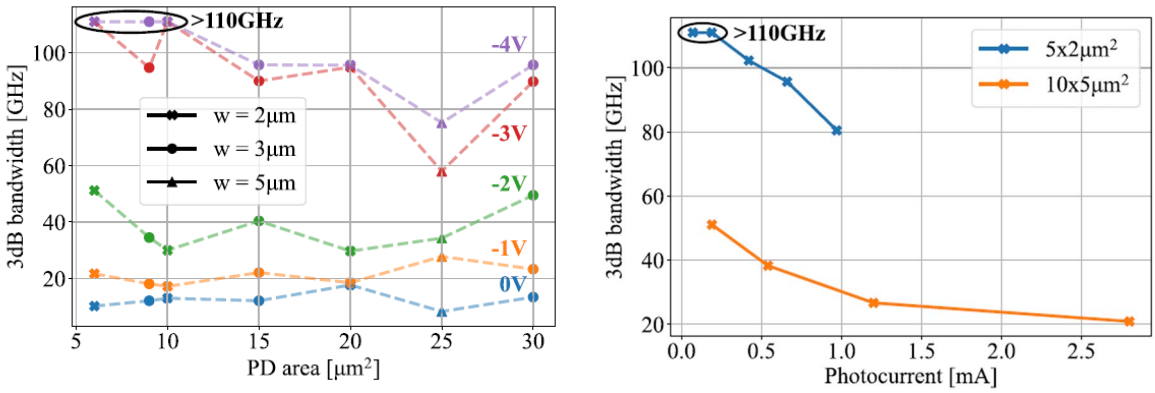

Figure 22: UTC-PD on an InP-membrane on-silicon platform

A concept of data transmission using the above UTC-PD design shows the BER in function of symbol rate (baud) for 4-PPM modulation with a net data rate of 117 Gb/s @ 50 Gbaud.

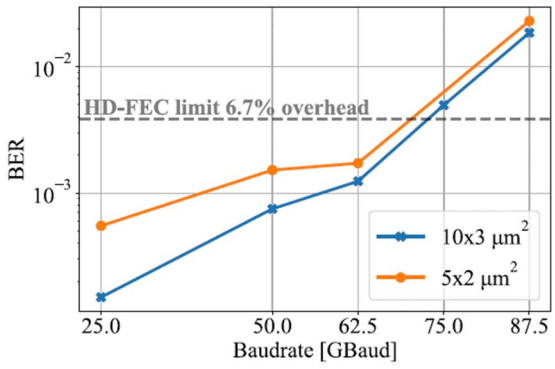

Figure 23: BER vs Gbaud for 4-PPM using two UTC-PD implementations

The measured 3 dB bandwidths (Figure 22) suggest transmission rates beyond 100 GBaud, which was however not achieved (Figure 23), due to the bandwidth reduction at the relatively high photocurrent operation point.

The mismatch in optimal photocurrent operation point between the bandwidth (UTC-PD operating alone) and responsivity (UTC-PD operating in conjunction with transmission chain circuits) is limiting the data transmission measurements due to an inferior signal-to-noise ratio at low photocurrent (high bandwidth) and reduced bandwidth at high photocurrent (high responsivity).

The significant progress in photonic-based THz generation still faces technical challenges to address.

7 Aspects of THz radio propagation

7.1 General

Channel models for THz communications and sensing depend on the frequency bands of interest, which in turn depend on the deployment scenario Next frequency bands are discussed.

7.2 Frequency bands

As mentioned in a previous clause, THz frequency ranges from 100 GHz to 10 THz (0,03 mm to 3 mm wavelength). Frequencies below the THz spectrum consist of the mm-wave spectrum and microwave spectrum. Those frequency bands are heavily utilized for many types of communication and radar applications. Above the THz spectrum consists of the near- and mid-infrared spectrum with applications such as spectroscopy, wellness, and brain stimulation.

Red light has a limited ability to penetrate the skull. Most red light gets absorbed by scalp tissue but does not reach the brain directly. Some medical studies suggest red light therapy may influence brain function indirectly, like stimulating nitric oxide production or other mechanisms, such as arteries.

However, the near-infrared spectrum shows better penetration depth through the skull. Consequently, the high spectrum of THz is more desirable for BCI considering medical implants. Nevertheless, for immediate practical applications, regulations should be considered.

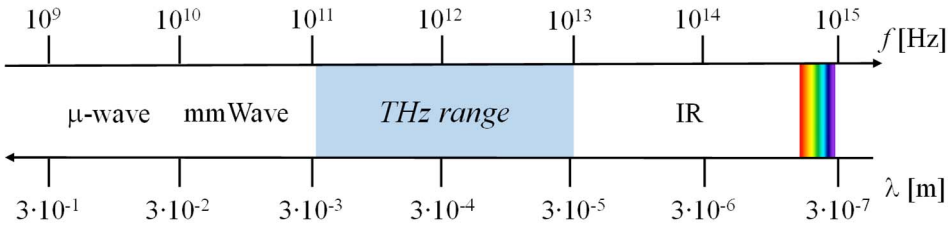

Figure 24: THz spectrum

Figure 25 shows the THz spectrum divided according to ITU-R Radio regulations.

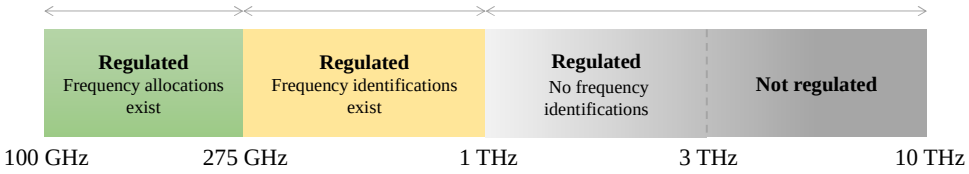

Figure 25: Current regulatory status of THz spectrum.

As discussed before, the ITU regulates the frequencies from 100 GHz to 3 THz as follows:

- The spectrum from 100 GHz to 275 GHz is already allocated for Fixed and Mobile services on a co-primary basis.
- The spectrum from 275 GHz to 1 THz has been identified for communications, radar applications, and passive services. However, future allocations will depend on the open-call studies by the ITU, encouraging protections for passive services like radioastronomy, and Earth observation.
- The spectrum from 1 THz to 3 THz may be used for active and passive services without a regulatory framework, similar to ISM bands.
- Above 3 THz no regulations exist.

Reported THz channel measurements may be classified as:

1) 100 GHz to 175 GHz.
2) 175 GHz to 250 GHz.
3) 250 GHz to 350 GHz.
4) Above 350 GHz.

As an initial approach for medical application in the THz band, the following frequency bands seem a good fit:

1) 100 GHz to 175 GHz: THz BANs (on-body applications).
2) 175 GHz to 250 GHz: Remote surgery.
3) 250 GHz to 350 GHz: BCI (in-body applications).
4) Above 350 GHz: BCI (in-body to off-body applications).

7.3 Channel modeling approaches

7.3.1 General

Conventional wireless systems design relies on accurate simulation of radio propagation effects or channel modeling. It provides insights into the behavior performance and dependability of wireless systems and consequently, it enables the development of innovative technologies. Considering electromagnetic propagation, where intricate interactions occur between electromagnetic waves and various objects (antennas, humans, obstacles), simulation results can predict signaling behavior, interference patterns, and channel characteristics. However, the accuracy and reliability of channel modeling rely on their alignment with real-world measurements.

7.3.2 Extension to ETSI TR 138 901 Study on channel model for frequencies from 0,5 GHz to 100 GHz

7.3.2.0 Introduction

The ETSI TR 138 901 [i.1] channel model document provides a probabilistic channel model for frequency bands ranging from 0,5 GHz to 100 GHz. It has been useful for designing, optimizing, and evaluating 5G system designs for various physical layer enhancements. It supports simple stochastic channel models (Tapped Delay Line models) and a more complex map-based hybrid channel model.

The ETSI TR 138 901 [i.1] TDL-based channel model generates transmitter (Tx) and receiver (Rx) antenna geometries based on 3D coordinate systems, generates Angles of Arrival (AoAs), Angles of Departure (AoDs), and delay parameters of multi-path components, according to statistical characteristics depending on scenarios, and then sums them up to generate time domain channel coefficients.

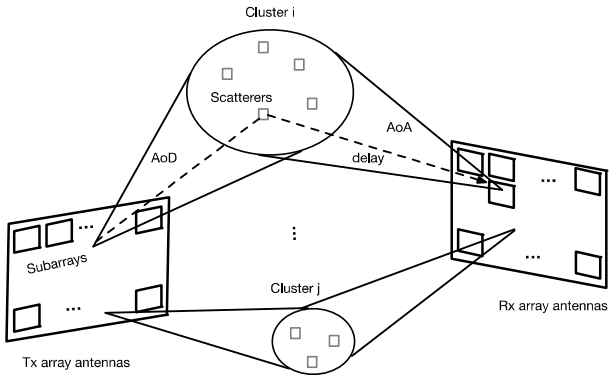

Figure 26: TDL-based channel model based on ETSI TR 138 901 [i.1])

Figure 26 shows the ETSI TR 138 901 [i.1] TLD-based channel model. It consists of a number of AoA/AoD/delay multipath components associated to generated clusters based on statistics. The channel coefficients are generated based on Tx and Rx array structures. Channel coefficients are generated using AoAs, AoDs, and delay values for multipaths without directly generating the locations or antenna geometry of scatterers (non-geometry-based stochastic model).

The ETSI TR 138 901 [i.1] channel models have the following limitations for THz applications:

1) Frequency range up to 100 GHz.
2) Planar wave modeling.
3) Handling of large bandwidths.
4) Lack of sensing channel modeling.

7.3.2.1 Frequency range up to 100 GHz

Statistical parameters and general TDL-based methodology should be revised for the THz spectrum, based on measurement campaigns or deterministic approaches, like ray tracing.

7.3.2.2 Planar wave modeling

The far-field region is defined by the Rayleigh distance as:

$$r \geq \frac{2D^2}{\lambda_c}$$

where D is the diameter of the antenna aperture, and λ_c is the wavelength of the carrier signal. If r is larger than this distance, then an antenna beam behaves like a spherical wave and starts to diverge.

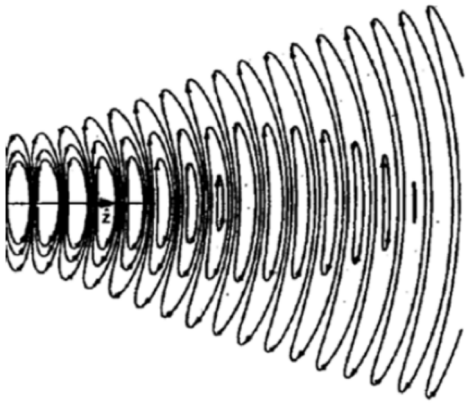

Figure 27: The right half of a Gaussian beam displays the physics of the near zone/field, the Fresnel zone, and the far zone/field. In the far zone, the field behaves like a spherical wave

Conventionally, a long-distance r is assumed that compared to the size of an antenna for frequencies below 100 GHz, the planar wave modeling (or far-field modeling) is acceptable. However planar wave modeling may be inaccurate for THz channel modeling since the communication distance may be less than the Rayleigh distance. In THz frequencies, the spherical assumption of wave propagation needs to be reconsidered.

Figure 28 illustrates the planar and spherical wave models. In the planar wave model, AoA and AoD are used to generate phase terms of channel coefficients, and the wave propagation distance is used to determine propagation delay. In the spherical wave model, each distance between each Tx-Rx antenna pair contributes to the phase and the delay of each channel coefficient. The far-field assumptions may not be applicable in THz bands and distance calculations between individual antenna pairs may be required.

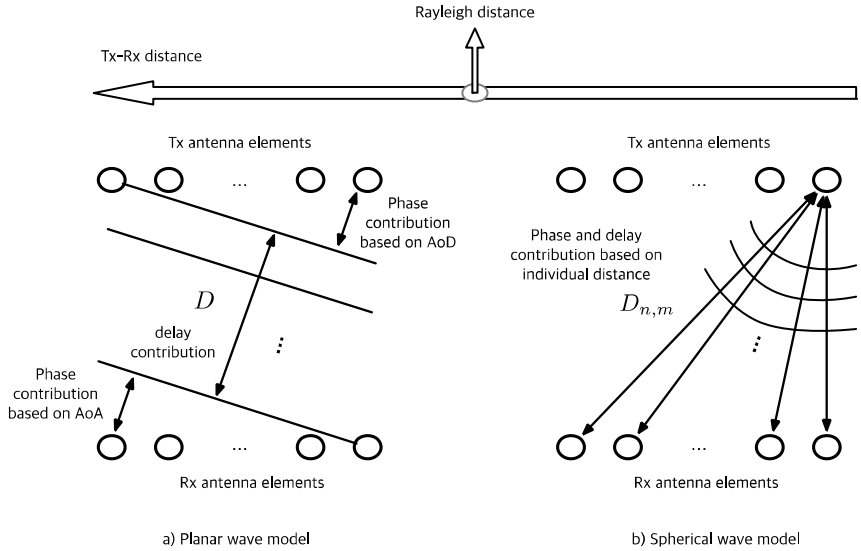

Figure 28: Planar and spherical wave models

7.3.2.3 Handling of large bandwidths

ETSI TR 138 901 [i.1] channel models use the carrier frequency f_c or wavelength λ_c for channel gain and/or phase calculation. Since the fractional bandwidth and/or aperture to wavelength ratio can be larger at THz compared to the lower frequency band, it is necessary to study the need for using a sub-band-specific center frequency, depending on the considered RF architecture.

7.3.2.4 Lack of sensing channel modeling

ETSI TR 138 901 [i.1] channel models were designed for links between the base station and UE and lacked the sensing channel model aspects. Sensing scenarios such as monostatic or bistatic sensing channels are not modeled, which makes them unsuitable for some THz use cases.

Sensing channel modeling extensions for the ETSI TR 138 901 [i.1] channel models may be classified as:

Mono-static sensing for coordinator and devices (on-body and in-body) sensing needs to be supported. Bi-static sensing: coordinator to device sensing needs to be supported. For these sensing scenarios, Large-Scale Parameters (LSPs) and Small-Scale Parameters (SSPs) are additionally defined for sensing channel generation. Depending on the type of target to be sensed and the use case, the altitude, LSP/SSP generation of the target or device may be different.

LOS/NLOS state determination for sensing channel. In most radar-based sensing channel modeling, it is assumed that a target exists (i.e. the channel between the target and the sensing device is LOS state). This may be sufficient for evaluating only sensing performance, but to evaluate performance from a system perspective and evaluate integrated sensing and communication performance, an actual channel model including NLOS between the sensing device and target is needed. The existing distance-dependent LOS/NLOS state decision probability model may be reused (in this case, the distance between the Tx device and the Rx device should be replaced with the distance between the sensing device and the target). Additionally, parameters such as Delay Spread (DS), Angular Spread (AS), Shadowing Factor (SF), Path Loss (PL), etc. may be determined differently depending on the LOS/NLOS state.

Large-Scale Parameters (LSPs) for the sensing channel: DS, AS, SF, PL, and Ricean K factor (K) can be different from those of the communication channel. Figure 29 shows an example of different angular spread/distribution in communication and sensing channels. In a communication channel, since the base station and the UE have different antenna heights, it is desirable to use different angular distributions for AoA and AoD. However, in the case of mono-static sensing, since the Tx and Rx are co-located and their antenna height are the same, the AoA and AoD should have the same distribution.

Frequency range limitation for sensing: ETSI TR 138 901 [i.1] channel models are limited to 100 GHz. For sensing in THz, the frequency range needs to be extended to THz bands.

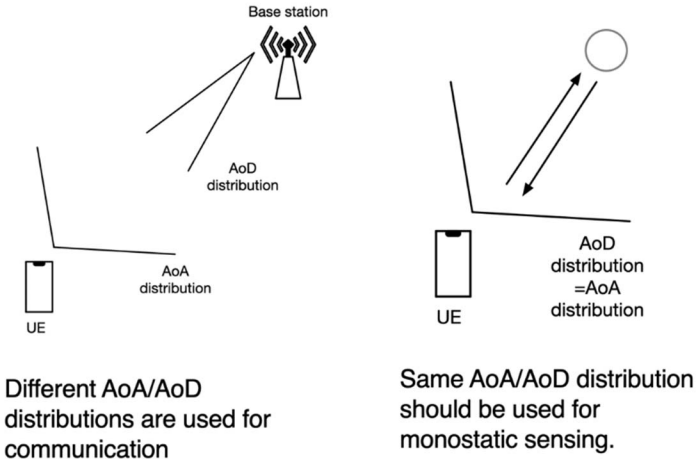

Figure 29: AoA and AoD distribution for communication and sensing

7.3.3 Molecular absorption

Molecular absorption may be an issue in THz bands. As it is known, the absorption coefficient depends on frequency giving the THz band a very peculiar frequency selective spectral absorption profile, such that the loss level for longer ranges can be larger since the radio waves go through more molecules. Thus, the molecular absorption modeling coefficients depend on distance and frequency. ETSI TR 138 901 [i.1] channel models propose to apply different molecular absorption modeling coefficients per cluster or Oxygen Loss (OL).

The molecular absorption loss function to the frequency-domain channel transfer function at each frequency point of $f_c + \Delta f$ within the considered frequency range $[f_c - B/2, f_c + B/2]$, where B is the bandwidth. In turn,

Alternatively, the molecular absorption loss for the *n*th path at the frequency of $f_c + \Delta f$ maybe modelled as:

$$L_n^{\text{molecular}}(f_c + \Delta f) = \alpha(f_c + \Delta f)c\tau_n$$

where c the speed of light, τ_n is the absolute propagation delay of the n-path, and $\alpha(\cdot)$ is the absorption coefficient, and frequencies under the considered bandwidth $[f_c - B/2, f_c + B/2]$, where B is the bandwidth.

In the THz spectrum supporting very wide bandwidths, frequency-selective molecular absorption coefficients should be considered. Another aspect is that different molecular absorption coefficients are applied per path. This is because the molecular absorption loss value is related to distance.

Another aspect of research is molecular absorption loss due to human tissues in the case of in-body applications.

7.3.4 Human Blockage

Human blockage has been studied extensively for millimeter-wave and sub-THz frequencies due to high attenuation and diffraction effects caused by human bodies. The shorter wavelengths at these frequencies are more susceptible to obstructions by small objects, including human bodies. To address these challenges, various modeling approaches have been developed, including Knife-Edge Diffraction (KED), the Uniform Theory of Diffraction (UTD), and Physical Optics (PO). KED, though simple and computationally efficient, lacks accuracy in complex 3D scenarios. UTD offers a balance between accuracy and computational efficiency, particularly when approximating human bodies with hexagonal shapes. PO provides the highest accuracy but at the cost of increased computational complexity, making it less scalable for large-scale scenarios.

Human blockage may play a significant role in the THz spectrum and for use cases like in-body to on-body applications, including BCI, BAN group communications, and remote surgery.

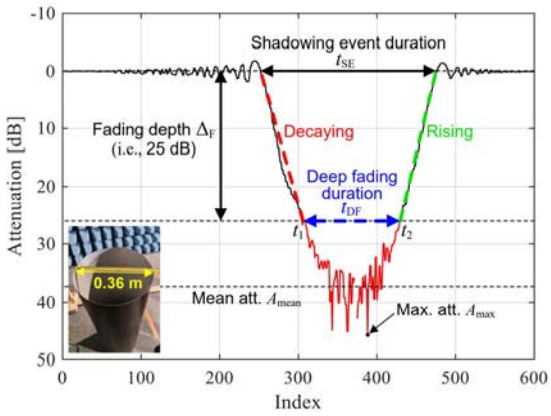

Figure 30: Fading pattern of a human modeled as a cylinder in 139 GHz to 141 GHz

7.3.5 Effect of THz radiation on skin

CWC University of Oulu conducted a measuring campaign to study the effect of THz radiation on human skin. Initially, pork chops were used as a proxy out of precaution, rather than using a human, for this initial experiment.

The pork's skin was separated as much as possible, as shown in Figure 31.

Figure 31: Pork chops skin samples

Although pork's skin may be a good approach to human skin, it is considered that it is dead tissue with more fat than an average human and without capillary veins blood flowing. The impact on the measurements is under evaluation.

The pork's skin was placed on the TeraPulse 4000 spectrometer with a modular sample compartment for transmission with a spectral range of 0,06 THz to 5,0 THz. Figure 32 shows the spectrometer covered in plastic for the protection of the instrument from the pork chop samples.

Figure 32: TeraPulse 4000 spectrometer from TeraView®

The pork skin samples were placed as shown in Figure 33.

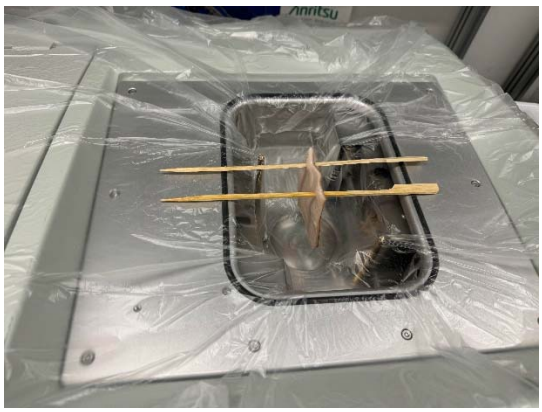

Figure 33: Experiment set up

The spectrometer was calibrated to transmit at 1 THz.

7.4 Propagation modelling

7.4.1 Spherical wave model

Conventionally, wireless systems assume operation in the far-field region, where propagation is modeled using the plane wave theory. However, this assumption may not be accurate for modeling THz propagation in short-distance links. Given the short wavelength relative to the effective antenna aperture, part of the coverage area can fall into the near-field region. Hence, the plane wave theory is not accurate enough and should be replaced by spherical wave theory (modeling spherical wavefronts).

Electromagnetic radiation from an antenna is divided into reactive near-field, radiating near-field, and far-field as illustrated in Figure 34.

a) In the reactive near-field region, the EM radiation exhibits a reactive behavior and is not fully radiated. Part of the energy can be deflected back to the source. In this region, the amplitude and phase distribution of the field depend on the distance from the antenna.

b) In the radiating near-field region (also called the Fresnel region), the EM field is fully radiated toward outer space, and its phase distribution depends on the radial distance from the antenna. A spherical wavefront model can represent it.

c) In the far-field region, the phase distribution of the EM field can be modeled as independent of the distance from the antenna. The radiated field is represented as a plane wave. Most wireless systems are designed assuming EM propagation in the far field.

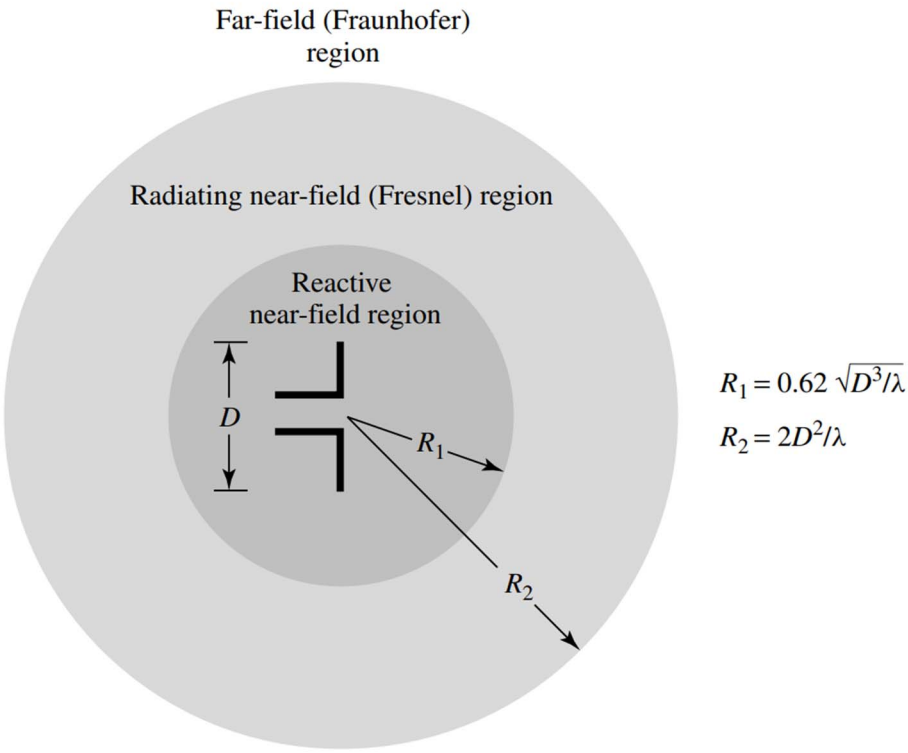

Figure 34: Electromagnetic radiation zones

In a clustering channel model, each path is associated with a wave vector **k**(x, y, *z*, *t*), which represents the phase variation of the propagating wave that is observed at the point (x, y, *z*) at epoch *t*.

In far-field conditions, EM waves are approximated as having a planar wavefront, which is constant and time invariant throughout the space and depends only on the AoD/AoA of the plane wave: $\mathbf{k}(x, y, z) = l, \ \forall(x, y, z)$.

In BCI devices (implanted or wearables) operating at short distances using small wavelength radio waves, an extension is required for modeling spherical wavefronts. The extension is to wireless channel models based on far-field radiation.

In the Fresnel region, the plane wave assumption is not valid anymore, and a spherical wavefront model should be used instead. In this case, the wave vector is no longer constant but varies in space.

In a stochastic approximation, the phase variation over the RX link. depends on the incident angle and position to the center of a spherical wavefront. Hence, conventional channel models can be extended to support the modeling of spherical wavefronts, where only the effects of the wave's curvature on the phase are considered. A geometric representation is shown in Figure 35.

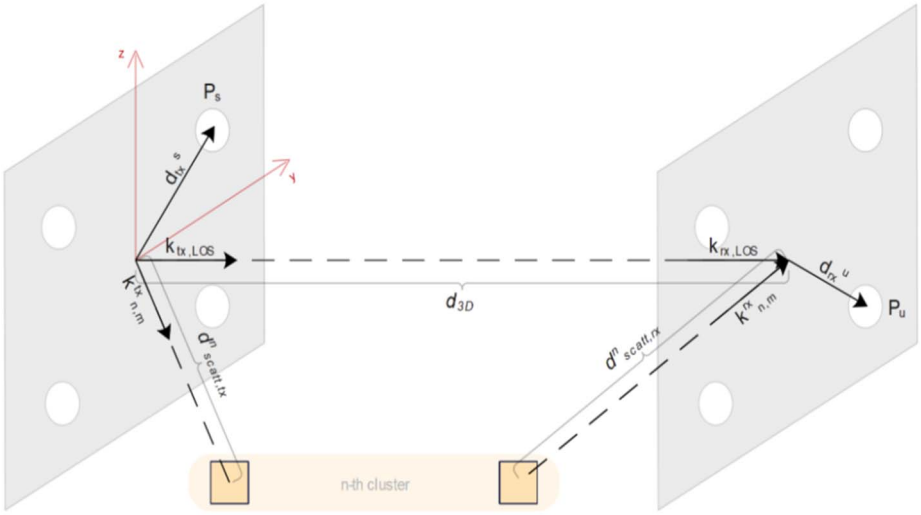

Figure 35: Spherical waveform moving

In the LOS component, the phase excitation component between the s-th transmit and the u-th receive elements is equivalent to their distance:

$$\begin{aligned}\Delta\Phi_{LOS}^{s,u} &= d_{3D} - ||P_s - P_u|| \\ &= d_{3D} - ||\mathbf{d}_{tx}^{s} - d_{3D} \cdot \mathbf{k}_{tx,LOS} - \mathbf{d}_{rx}^{u}||,\end{aligned}$$

In the NLOS component, the center of the spherical wavefront corresponds to the position of the first (in case of the departing wave) or last (in case of the arriving wave) scatterer, as represented in Figure 35. The phase excitation can be expressed as:

$$\Delta\Phi_{tx,n,m}^{s} = d_{scatt,tx}^{n} - ||d_{scatt,tx}^{n} \cdot \mathbf{k}_{tx,n,m} - \mathbf{d}_{tx,s}||$$
$$\Delta\Phi_{rx,n,m}^{u} = d_{scatt,rx}^{n} - ||d_{scatt,rx}^{n} \cdot \mathbf{k}_{rx,n,m} - \mathbf{d}_{rx,u}||$$

In this manner, the spherical wave model can be incorporated via the phase variation of LOS and NLOS components into a conventional channel model generator.

8 Aspects of THz hardware interfaces

8.1 ADC and DAC

Digital Converters are the bridge between the digital baseband signal domain and the analog radio frequency signal domain. Hence, the performance of data converters can be a bottleneck for the whole system. As the transmission bandwidth in THz bands can be large, the requirements for the speed of data converters increase considerably. Also, the power consumption of data converters grows exponentially as the resolution increases. Therefore, the trade-offs between power consumption, speed, and precision should be carefully considered. For example, sub-THz transceivers with a bandwidth of 10 GHz would require baseband data converters with sampling rates of at least 20 GS/s.

Data converters have multiple parameters that are necessary to characterize and understand their impact on the overall system performance. Those include resolution, sampling rate, noise, jitter, phase noise, distortion parameters, gain error, offset, and full scale. The following clause discusses the most critical parameters that determine the feasibility and performance capabilities of the data converter for high-speed applications.

The Walden Figure of Merit (FOM_W) is a normalized performance metric that represents the efficiency of the converter for its performance and captures the performance/speed/power trade-off with reasonable accuracy:

$$FOM_W(\text{in J/conv. step}) = \frac{Power}{2^{ENOB} \cdot f_s};\ NO = \frac{SNDR - 1{,}76}{6{,}02}$$

Where P is the power dissipation, fs is the Nyquist sampling rate, and ENOB is the effective number of bits defined by the Signal-to-Noise and Distortion Ratio (SNDR).

The FOM_W relates the ADC power dissipation to its performance, represented by sampling rate and conversion error amplitude. Vendors report *FOM* annually for its best values in function of Delta-Sigma Modulators (DSMs) and Nyquist ADCs. The FOM_W assumes the power increases linearly with the sampling rate and exponentially with the effective number of bits. A smaller FOM_W indicates a more efficient ADC.

Another *FOM* that is suitable for noise-limited converters was proposed by Schreier:

$$FOM_S(\text{in dB}) = DR + 10\log_{10}\left(\frac{BW}{Power}\right)$$

Where *DR* is the dynamic range defined as the input range from full-scale to where the SNR reduces to 0 dB. This is typically a measure of the SNR in the absence of a signal, excluding large signal effects, jitter, and non-linearity. *BW* is the bandwidth of the ADC that the *DR* holds. A larger FOM_S indicates a more efficient ADC.

A modification of the Schreier *FOM* was proposed to capture the distortion, jitter, high-frequency impairments, and large-signal effects:

$$FOM_{S\_HF}(\text{in dB}) = SNDR' + 10\log_{10}\left(\frac{f_S/2}{Power}\right)$$

Where the *SNDR'* is the *SNDR* that captures largest signal, distortion, and jitter effects. The parameter f_s represents the sampling rate in Nyquist converters. For Delta-Sigma and other noise-shaped converters, f_s is the effective sampling rate, which is double the bandwidth over which the *SNDR* holds. A larger FOM_{S_HF} indicates a more efficient ADC.

The Walden FOM and the modified Schreier *FOM* are widely used to compare the efficiency and performance of data converters. As the sampling rate increases, converters tend to be less efficient. That is: the FOM is not fixed and tends to degrade with increasing speed for sampling rates above 100 MHz. This is an important consideration when attempting to extrapolate power and performance at different sampling rates.

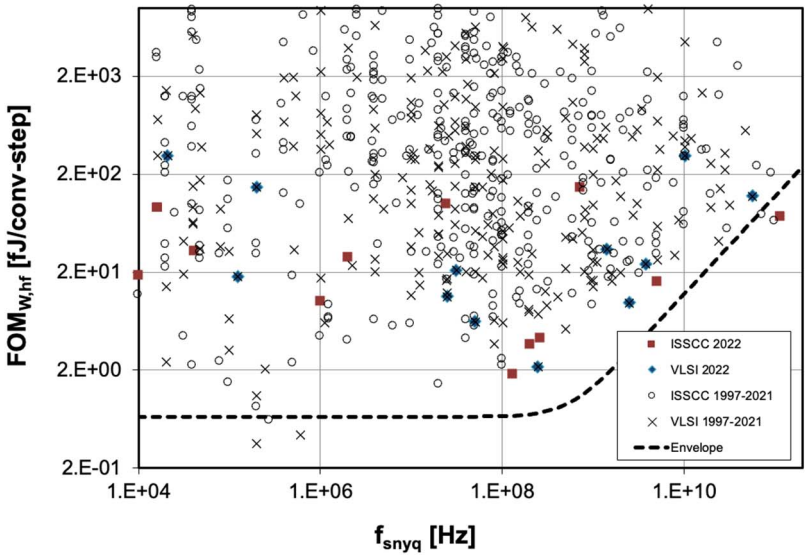

Figure 36: FOM_W versus sampling rate f_s

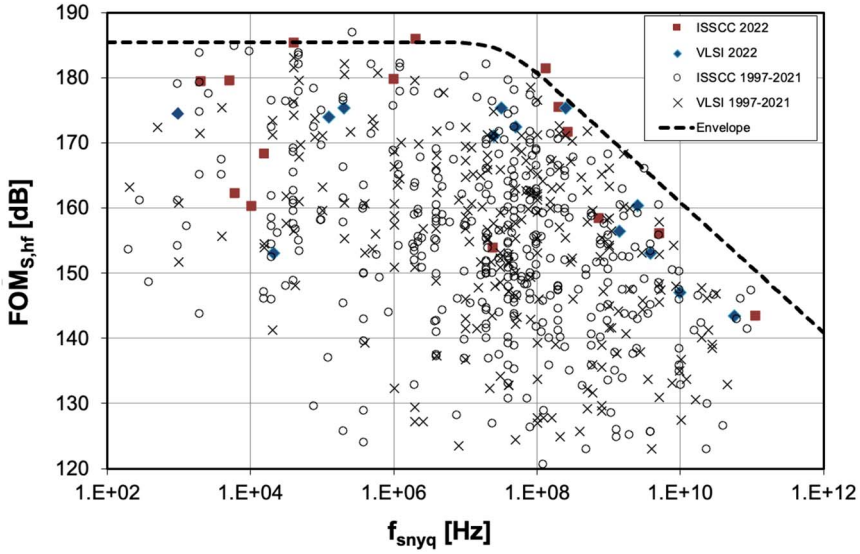

Figure 37: *FOM*$_{S\_HF}$ versus sampling rate f_s

As shown in Figure 36 and Figure 37, data converters with resolutions in the order of 4 to 6 bits and sampling rates in the order of 10 to 50 GS/s, consume power of about 50 mW to 100 mW with a Walden FOM of 40 to 60 fJ/step and modified Schreier FOM of 146 dB to 148 dB. Higher resolutions are achieved in the 10 GS to 24 GS/s range for higher power.

For example, 7 to 8 bits of performance consumes power in the range of 0,6 W to 1,5 W with a Walden FOM of about 180 fJ to 350 fJ/step and a Schreier FOMS of 146 dB to 148,5dB.

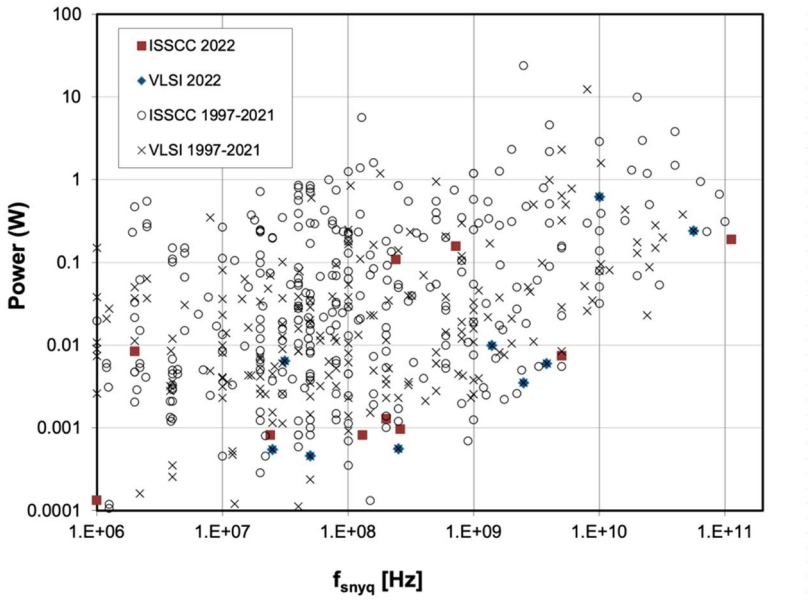

Figure 38: ADC power consumption versus sampling rate f_s

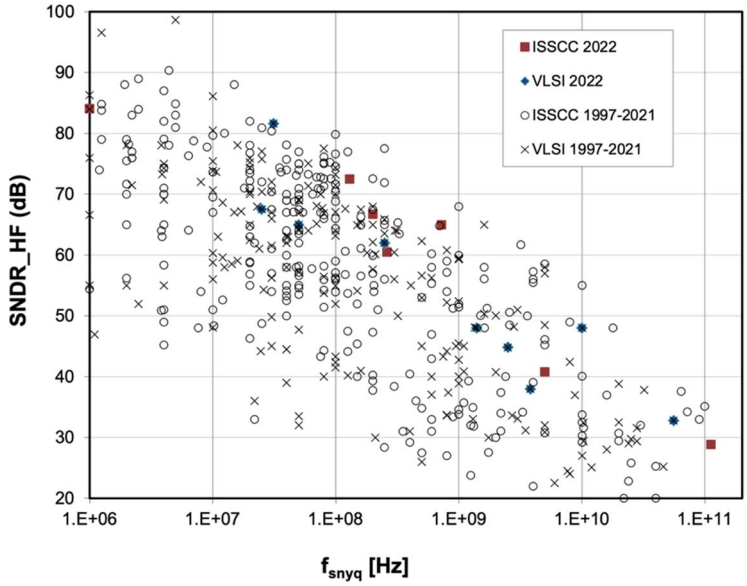

Figure 39: ADC high-frequency *SNDR* versus sampling rate f_s

Figure 40 shows the current trend of performance between resolution (SNDR) and sampling rate. The slope describes the frontiers of the state-of-the-art techniques and the trade-off between sampling rate and resolution. In THz bands, the sampling rate of data converters is typically very high (from tens of GS/s to hundreds of GS/s). However, data converters can only achieve relatively low resolution.

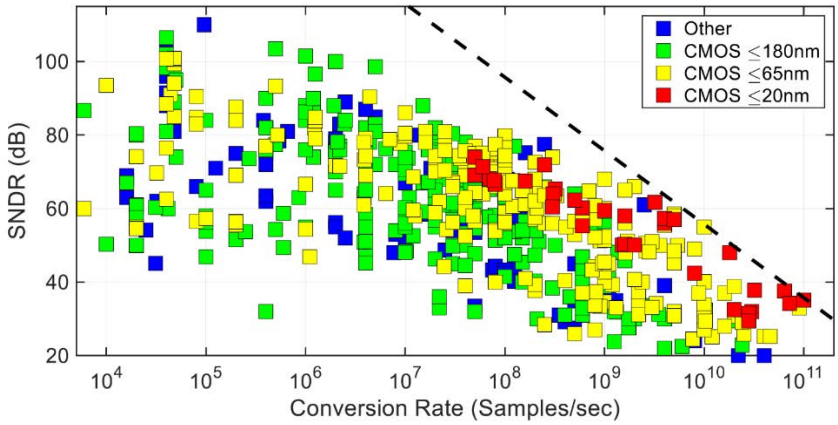

Figure 40: 20 Resolution versus sampling rate for different types of data converters

In addition to sampling rate and noise, the IMD3 and SFDR are the most important parameters used to characterize DACs (see Figures 41 and 42).

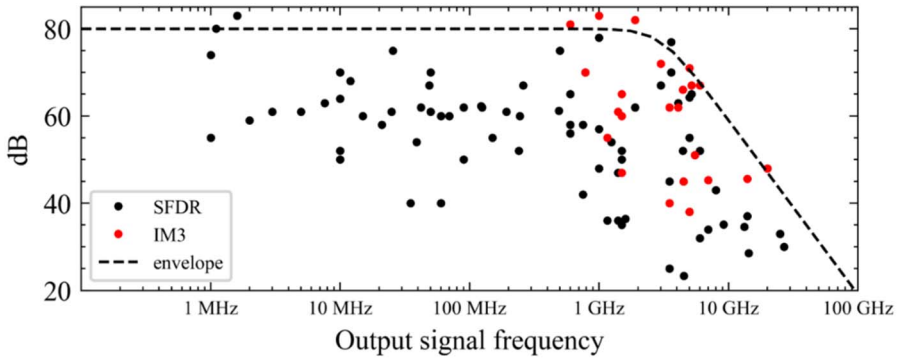

Figure 41: DAC Spurious-Free Dynamic Range (SFDR) and Third-order intermodulation products (IM3) vs output signal frequency

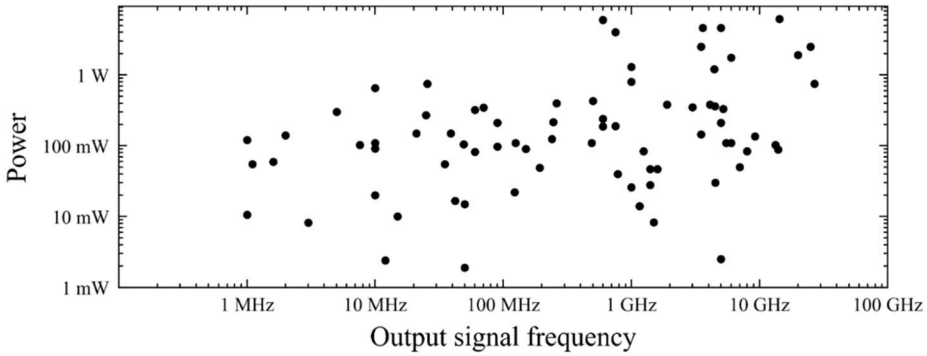

Figure 42: DAC power consumption versus output signal frequency

8.2 Sub-THz transceivers based on photonics

The state of the art on sub-THz transceiver architectures follows three architectures:

1) Sub-THz transmitter with an external optical modulator based on intensity modulation and a sub-THz receiver based on envelope detection.

2) Sub-THz transmitter and a sub-THz receiver architecture using direct modulation and envelope detection.

3) Sub-THz transmitter with an optical IQ modulator based on field modulation and a sub-THz receiver with a mixer based on coherent detection.

Figure 43 shows a sub-THz transmitter with an external optical modulator based on intensity modulation and a sub-THz receiver with a diode detector based on envelope detection. The data modulation is composed of two light sources (Laser Diode (LD)), an external optical modulator, an optical amplifier, and an optical bandpass filter. Two light sources are employed for the optical heterodyne mixing procedure. One LD is the optical Local Oscillator (LO), and the other LD is for optical intensity modulation. Based on the optical heterodyne mixing principle, the frequency difference between 2 light sources is converted to the output frequency of the photo mixer.

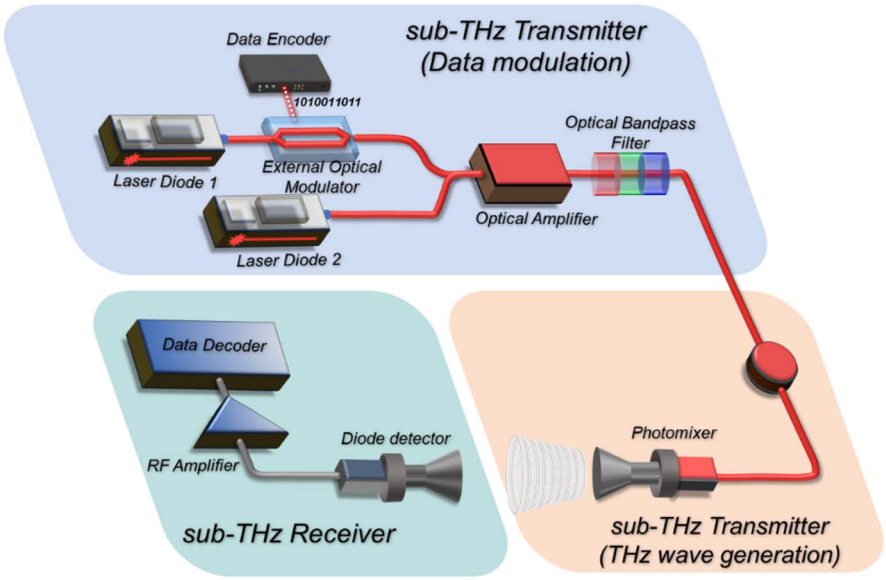

Figure 43: Sub-THz transceiver first method

Figure 44 shows a sub-THz transmitter and a sub-THz receiver architecture using direct modulation and envelope detection. This transmitter/receiver architecture is very similar to the configuration shown in Figure 43, but instead of using an external optical modulator, a directly modulated LD is employed as a light source and data modulator simultaneously. This configuration reduces the cost of the sub-THz transmitter. However, the modulation bandwidth of the directly modulated LD limits the data transmission speed. Currently, when using commercial directly modulated DFB-LD, the maximum transmission speed based on the OOK modulation format is known to be limited to 25 Gb/s.

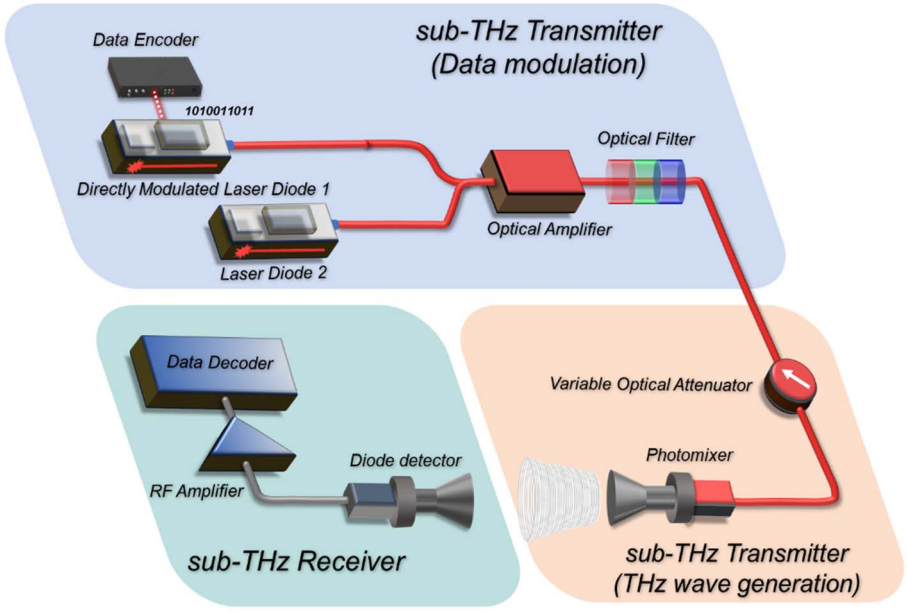

Figure 44: Sub-THz transceiver second method

Figure 45 shows a sub-THz transmitter with the optical IQ modulator based on field modulation and a sub-THz receiver with a mixer based on coherent detection. This transmitter/receiver architecture is similar to the configuration of Figure 1, but instead of using an optical intensity modulator for data modulation, it uses an optical IQ modulator that modulates intensity and phase simultaneously. Commercial optical IQ modulators support rates up to 40 G-symbols/s. The data encoder provides the I and Q signaling. The sub-THz receiver employs a coherent detection consisting of a mixer, frequency multiplier, and Local Oscillator (LO). The implementation cost of a sub-THz transmitter and a sub-THz receiver is relatively high and complex compared to the previous architectures. However, this configuration enables the transmission of multi-level signaling and multi-phase modulation/demodulation with high spectral efficiency. It results in transmission speeds of about 100 Gb/s or higher. It also provides the advantage of having a wide dynamic range for received signals due to coherent detection.

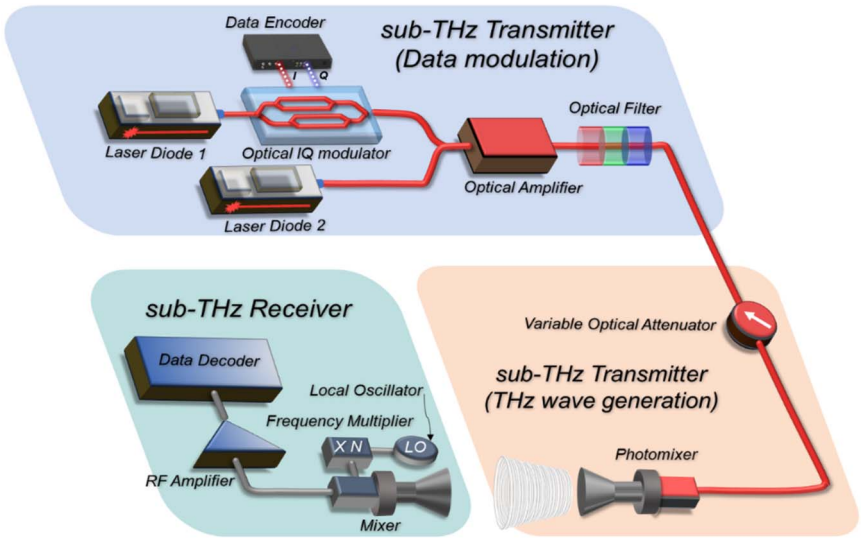

Figure 45: Sub-THz transceiver third method

8.3 Radio interface impairments

Towards experimental evaluations, previous clauses help to understand the impact of the use of radio interfaces on THz links in BCI applications.

Further studies describing impairment models are as follows:

a) Linear distortion is modeled by an FIR filter with a given transfer function. Power amplifiers and mixer characteristics are taken from the literature. Two filters are implemented dealing separately with the I/Q components, to consider that the mixer acts separately on the I and Q components.

b) Non-linear distortion is modeled by the AM/AM characteristic and the AM/PM characteristic.

c) In-phase and quadrature imbalance is modeled assuming frequency-independent impairments and realistic characteristics from the literature.

d) Phase noise is modeled using a realistic phase noise power density spectrum from the literature.

Research is in progress on the viability of using photonics systems.

Annex A:
Biological effects of THz radiation

A.1 DNA damage

There is considerable work on THz applied to cancer research. Mostly for its penetration properties and the hope of using it to detect tumors close to the skin.

Regarding DNA damage, THz radio waves are not ionizing radiation like X-rays and UV rays. THz radio waves are not energetic enough to break chemical bonds or ionize atoms or molecules. Hence, it is counterintuitive to think of DNA damage, and yet some publications claim so.

However, the evidence that THz radiation damages biological systems is mixed. Some studies reported significant genetic damage, while others, although similar, showed none.

Research aimed to address this discrepancy proposed a model that showed resonant effects allow THz waves to unzip double-stranded DNA, creating bubbles in the double strand that could significantly interfere with processes such as gene expression and DNA replication. That was in 2009. Since then, there has been no consensus on DNA damage by THz radiation. A number of publications claim that THz induces DNA damage, others, not at all, others maybe, and others THz enhances DNA damage repair.

It seems the reported biological effects of THz depend on many variables: frequency, power, experimental setup, and even teams: physicians, biologists, physicists, and electrical engineers show different findings.

A partial list of publications:

1) "High Power THz Activities at Seoul National University", G.S. Park et al.

2) "Effects of high-intensity non-ionizing terahertz radiation on human skin fibroblasts", Dmitry Sitnikov et al.

3) "Intense THz pulses cause H2AX phosphorylation and activate DNA damage response in human skin tissue", Lyubov V. Titova et al.

4) "THz exposure affects primary hippocampus neuron gene expression via alternating transcription factor binding", Sen Shang et al.

5) "No DNA damage response and negligible genome-wide transcriptional changes in human embryonic stem cells exposed to terahertz radiation", A. N. Bogomazova et.al.

6) "THz irradiation reduces the DNA damage marker γH2AX in human cells: THz wave enhances DNA damage repair?", Yuya Ueno et.al.

THz radiation (0,1 THz to 10 THz) is considered non-ionizing. This means that THz photons do not carry enough energy to directly break chemical bonds or ionize atoms and molecules, including DNA.

However, the question of whether THz radiation can alter human DNA is complex and has been the subject of ongoing research. Here's a breakdown:

- **Non-Ionizing Nature of THz Radiation:**
  - THz photons have energies in the range of 0,4 meV to 40 meV, which is much lower than the energy required to ionize biological molecules (typically several electron volts, eV).
  - Because of this low energy, THz radiation is not expected to cause direct DNA damage, such as single- or double-strand breaks, in the way that ionizing radiation (e.g. X-rays or gamma rays) does.
- **Research Findings:**
  - In Vitro Studies: Some laboratory studies on cells exposed to THz radiation have reported changes in gene expression, DNA repair mechanisms, or cell proliferation. However, these effects are often observed at **high power levels** or **prolonged exposure** times, which may not be representative of real-world conditions.

- In Vivo Studies: Research on living organisms, including humans, is limited. Most studies have not found significant evidence of DNA damage or harmful biological effects at typical exposure levels.
- Controversial Results*:* Some studies suggest potential biological effects, while others find no significant impact. The variability in experimental conditions (e.g. frequency, power, exposure duration) makes it difficult to draw definitive conclusions.

- **Safety Standards and Guidelines:**
  - Regulatory bodies, such as the International Commission on Non-Ionizing Radiation Protection (ICNIRP), have established safety guidelines for exposure to electromagnetic fields, including THz radiation.
  - These guidelines are based on the thermal effects of THz radiation and aim to prevent excessive heating of tissues. As long as exposure remains within these limits, THz radiation is considered safe.
- **Current Consensus:**
  - The majority of scientific evidence suggests that THz radiation, at typical exposure levels, does not directly alter human DNA or pose significant health risks.
  - However, more research is needed to fully understand the long-term effects of THz exposure, especially as THz technologies become more widespread in applications like imaging, communication, and security.
- **Areas for Further Research**
  - Long-term exposure studies to assess potential cumulative effects.
  - Investigation of low-power, chronic exposure scenarios.
  - Exploration of potential non-thermal mechanisms of interaction with biological systems.
- **Conclusion**
  - In summary, THz radiation is unlikely to directly alter human DNA due to its non-ionizing nature. However, indirect effects, such as thermal stress or oxidative damage, cannot be entirely ruled out and warrant further investigation. Current safety guidelines aim to minimize risks, but ongoing research is essential to ensure the safe use of THz technologies.

Annex B: Bibliography

- ETSI TS 103 325 (V1.1.1): "Smart Body Area Network (SmartBAN); Low Complexity Medium Access Control (MAC) for SmartBAN".
- ETSI TS 103 326 (V1.2.1): "Smart Body Area Network (SmartBAN); Enhanced Ultra-Low Power Physical Layer".
- ETSI 103 378: "Unified data representation formats, semantic and open data model".
- ETSI TR 103 719: "Guide to Identity-Based Cryptography".
- Chong Han et al.: "Terahertz Wireless Channels: A Holistic Survey on Measurement, Modeling, and Analysis", IEEE Communications Surveys & Tutorials, vol. 24, no. 3, third quarter 2022.
- Ericsson: "Microwave backhaul beyond 100 GHz," Ericsson Technology Review, February 2017.
- L. Liebermeister et al.: "Optoelectronic frequency-modulated continuous-wave terahertz spectroscopy with 4 THz bandwidth", Nature Communications, vol. 12, p. 1071, 2021.
- T. Ishibashi and H. Ito: "Uni-Traveling Carrier Photodiodes: Development and Prospects,", IEEE Journal of Selected Topics in Quantum Electronics, vol. 28, no. 2, pp. 1 to 6, March-April 2022.
- C. Castro et al.: "32 GBd 16QAM Wireless Transmission in the 300 GHz Band using a PIN Diode for THz Upconversion", Optical Fiber Communications Conference and Exhibition (OFC), pp. 1 to 3, 2019.
- I. Dan, G. Ducournau, I. Kalfass et al.: "A 300-GHz Wireless Link Employing a Photonic Transmitter and an Active Electronic Receiver With a Transmission Bandwidth of 54 GHz", IEEE Transactions on Terahertz Science and Technology, vol. 10, no. 3, pp. 271 to 281, May 2020.
- B. Gashi et al.: "Broadband 400-GHz InGaAs mHEMT Transmitter and Receiver S-MMICs", IEEE Transactions on Terahertz Science and Technology, vol. 11, no. 6, pp. 660 to 675, November 2021.
- D. Ahn et al.: "Optimal design of wireless power transmission links for millimeter-sized biomedical implants", IEEE Transactions on Biomedical Circuits and Systems 10 (1) (2016).
- ETSI GR THz 002 (V1.1.1): "TeraHertz technology (THz); Identification of frequency bands of interest for THz communication systems".

Annex B:
Change history

Date	Version	Notes
December 2022	0.0.1	Release of an early draft.
August 2025	1.1.1	First published version.

History

Document history		
V1.1.1	August 2025	Publication